Development of Meteorological Data Explorer for Windows

Jiye ZENG[1], Masayuki KATSUMOTO[2], Reiko IDE[2], Michiko INAGAKI[2],
Hitoshi MUKAI[2] and Yasumi FUJINUMA[2]
[1]Global Environmental Forum, 16-2 Onogawa, Tsukuba, Ibaraki, 305-8506 Japan
[2]Center for Global Environmental Research, National Institute for Environmental Studies
16-2 Onogawa, Tsukuba, Ibaraki, 305-8506, Japan

Abstract

The Meteorological Data Explorer is a software developed for Windows and comprises a tool to calculate air trajectory and a tool to extract and display meteorological data of European Center for Medium-Range Weather Forecast. It is the successor of the Global Meteorological Data Display System developed for the UNIX platform. The objective of developing the Meteorological Data Explorer as a component of the Data Analysis and Graphic Display System is to eradicate the barrier between user and the supporting system, which was exclusively UNIX before this development. Using the software users can conduct trajectory calculation or data extraction from their own desktop. The new program improves the performance of trajectory calculation dramatically.

Keywords: Meteorological Data, Air Trajectory, Trajectory Model and Quality

1. Introduction

1.1 Development Histrory

Atmospheric trajectory programs became available in the mid 1970s (Heffter and Taylor, 1975; Pack et al., 1978); and were used commonly to gain better understandings of airflow patterns around observatories (Miller, 1981a, 1981b; Merrill et al., 1985; Harris, 1992; Harris and Kahl, 1990, 1994), to investigate variations of observed chemicals in relation to airflow (Harris et al., 2000), and to identify the source regions of pollutants (Moody and Galloway, 1988; Polissar et al., 2001). Until early 1980s, trajectory calculations were done on constant pressure surfaces, commonly referred to as isobaric trajectory model. The Gridded Atmospheric Multilevel Backward Isobaric Trajectories program by the Geophysical Monitoring for Climate Change of NOAA (Harris, 1982) is an example of early trajectory programs. Other types of trajectory models were then scarcely available because of limited vertical levels of meteorological data and limited computer resources. It was experimentally approved (Kuo et al., 1985; Haagenson et al., 1987) that trajectories resulted from the isobaric model, which neglects the vertical transport, was not as good as those obtained from the isentropic model (transport on the surface of constant potential temperature) and 3D-wind model (estimating transport from 3D-wind field). These two models are commonly included in recent trajectory programs. The HYSPLIT of NOAA (Draxler and Hess, 1998) and the FLEXTRA of the University of Munich (Stohl, 1999) are two of the free trajectory programs.

In response to the increasing demand for trajectory program as a tool for interpreting variations of observed data from atmospheric monitoring, the Center for Global Environmental Research (CGER), National Institute for Environmental Studies (NIES) started the development of the Global Meteorological System (GMET) in 1994 based on Hayashida's large scale computing system for the host computer HITAC M280 of NIES (Katsumoto et al., 2002). The system includes an isentropic and an isobaric model and allows users to calculate trajectories either by batch processing or through a graphic user interface. The system also includes graphic tools to display meteorological parameters in the dataset of European Center for Medium-Range Weather Forecast (ECMWF) and to plot data of atmospheric observations. However, the following problems remain after many modifications by the developer:

- Trajectory computing is slow. On the SUN Workstation Ultra-10, GMET takes about one minute to produce a three-day backward trajectories. One of the main factors that affect GMET's performance is the loading and decoding of ECMWF data. When the program was transplanted from HITAC M280 to the SUN Workstation in 1994 available computer memory was still limited. As a result, the program had to be designed to read and decode a small piece of ECMWF data at a time, and access the same file several times in an integration from one available data file time to another (based on personal communications with N. Furuhashi).
- Because of the limitation of the absolute pressure coordinate, the isentropic model of GMET failed frequently in calculating trajectories at low altitudes where the isentropic surface may intersect the earth's surface. Although the isobaric model does not have this problem, trajectories produced by isobaric assumption are not as realistic as those by isentropic assumption (Kuo et al., 1985; Haagenson et al., 1987). Besides, a trajectory has undefined physical meaning when it goes through mountains, which occurs frequently in isobaric model if the starting position is near or over a continent and the starting altitude is close to the surface.

- Using GEMT in the batch mode is rather difficult for novice computer users, partly because of the complexity of UNIX. Although GMET has a GUI component for single trajectory, computing multiple trajectories through the GUI is quite tedious and impractical.

These problems led to the development of the Meteorological Data Explorer (METEX) for Windows. In the beginning of METEX's development, the author tried to adopt FLEXTRA (source code available), but found it difficult partly because FLEXTRA expects the ECMWF data on the grids of ECMWF's operational model, whereas the ECMWF data maintained by CGER have been interpolated to the absolute pressure coordinate. For using HYSPLIT (compiled binary only), meteorological data must be converted to a format specific to HYSPLIT. Without the source code, it is very difficult to ensure correct conversion of meteorological data and to modify the program when necessary. The development history of METEX/GMET is summarized in Figure 2.

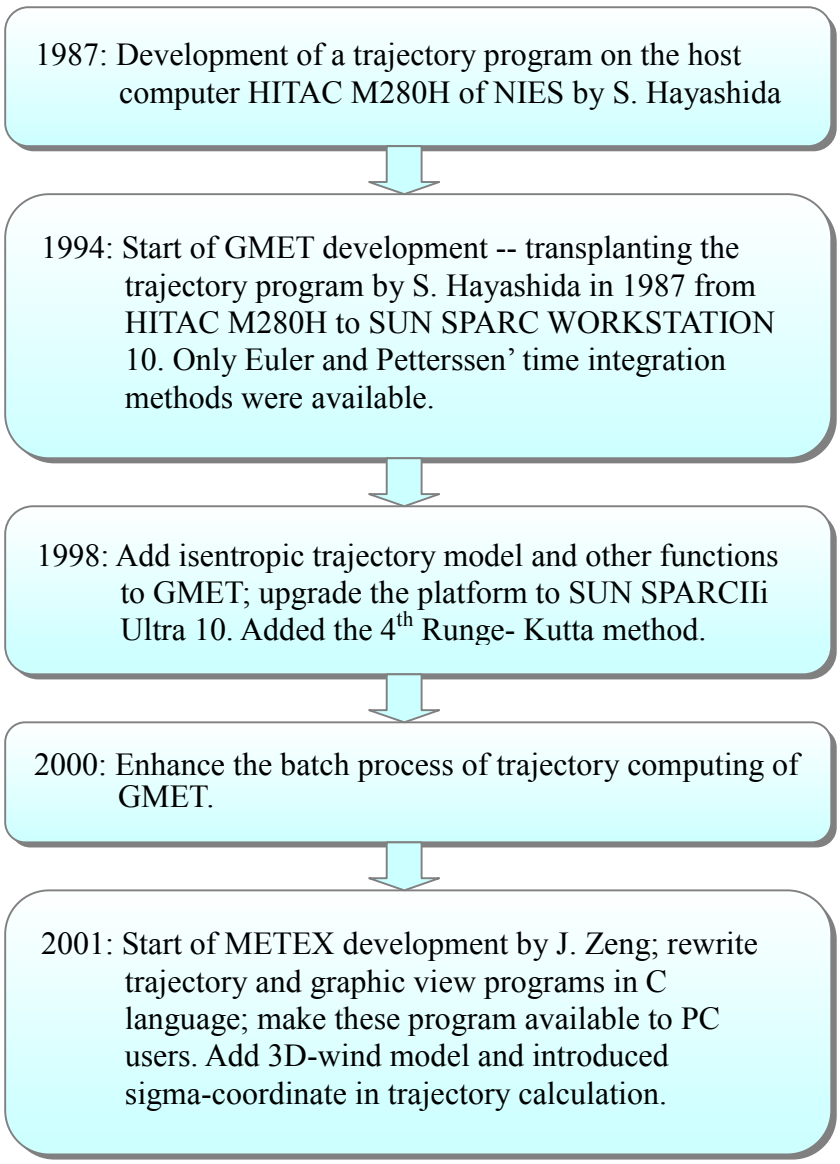

Figure 2 Development history of METEX/GMET in CGER.

1.2 Functions of METEX

Users can use METEX to calculate backward and forward trajectories of air parcels (Figure 3) and view trajectory-related meteorological parameters (Figure 4) in the ECMWF database by personal computers (PC) that have Windows 95®, 98®, ME®, NT®, 2000®, or XP® installed. A client PC connects to the central database server through LAN to fetch ECMWF data and do the rest of the computing using its own CPU power (Figure 5). This design makes it possible to access the same meteorological database simultaneously by multiple PCs from different offices in NIES, and therefore offers a great flexibility and convenience to researchers.

Flexibility and convenience are not the only advantage of METEX over other programs of the same kind. The speed of trajectory computing of METEX is surprisingly fast comparing with most, if not all, available trajectory programs. For example, a PC with one GHz CPU power (a common configuration at the time of METEX's development) can produce more than 150 lines of 3-day backward trajectories in one minute. The author of the program has taken great considerations in optimizing the performance and minimizing the memory consumption of METEX. Novice computer users will appreciate the easy-to-use graphic user interface, which is not commonly available in other programs, especially in those written for UNIX platforms. In addition, it takes less than 1 MB of memory to run the conversion program, less than 3 MB to run the display program, and about 6 MB to run the trajectory program. Features of METEX and GMET are listed in Table 1.

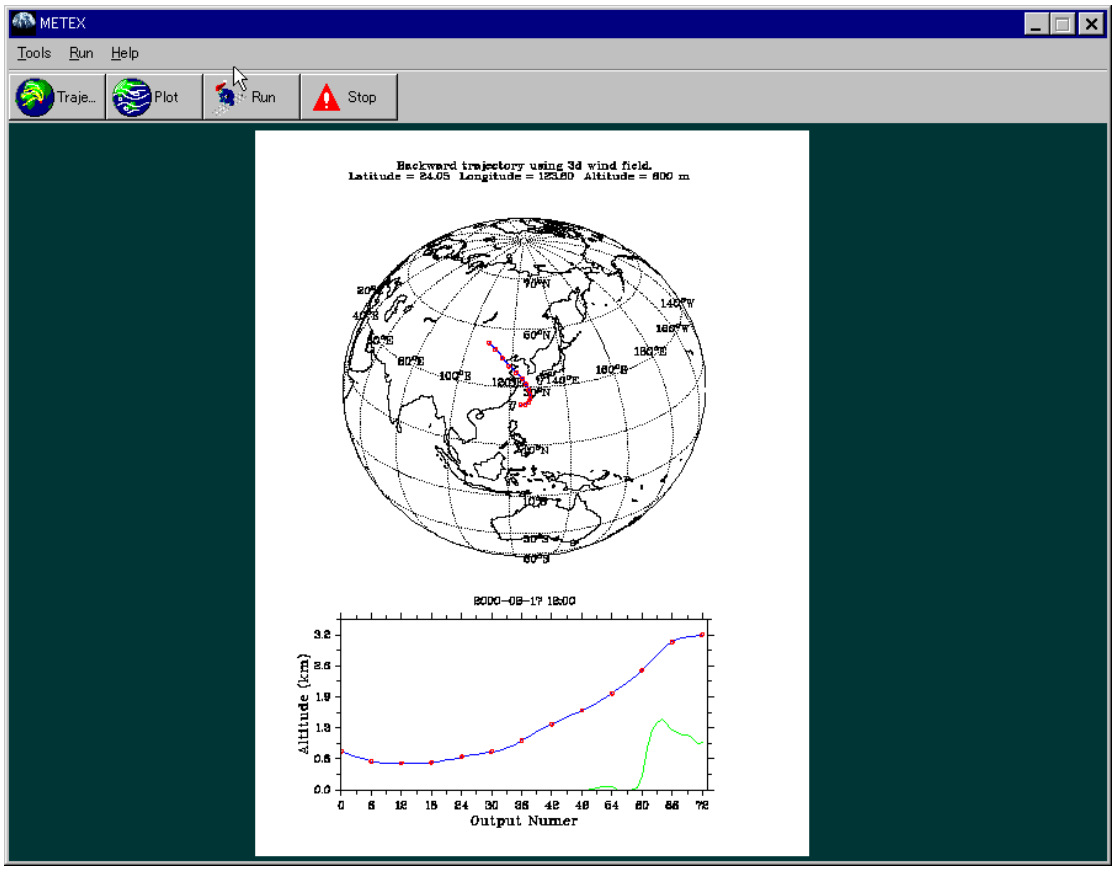

Figure 3 Calculate trajectory by METEX.

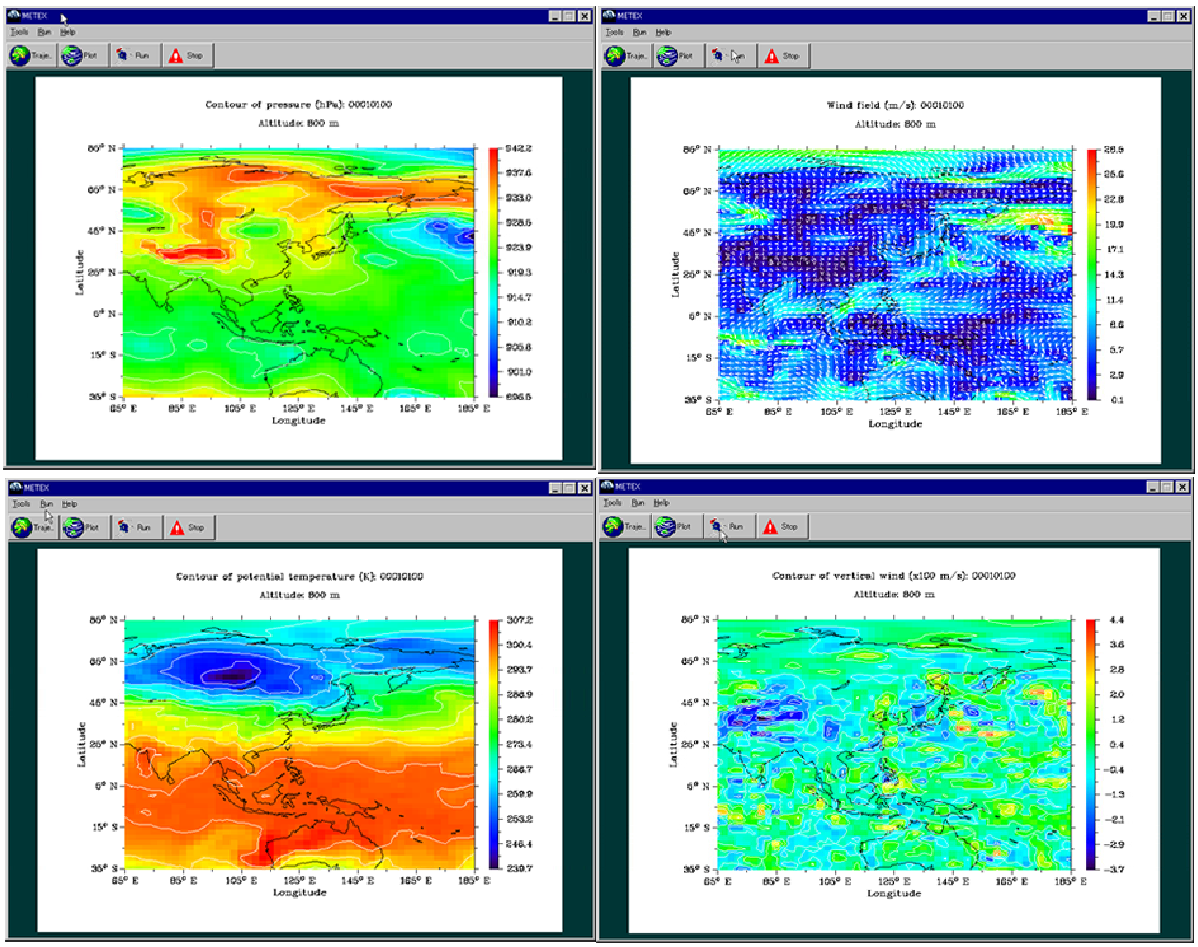

Figure 4 View ECMWF parameters by METEX.

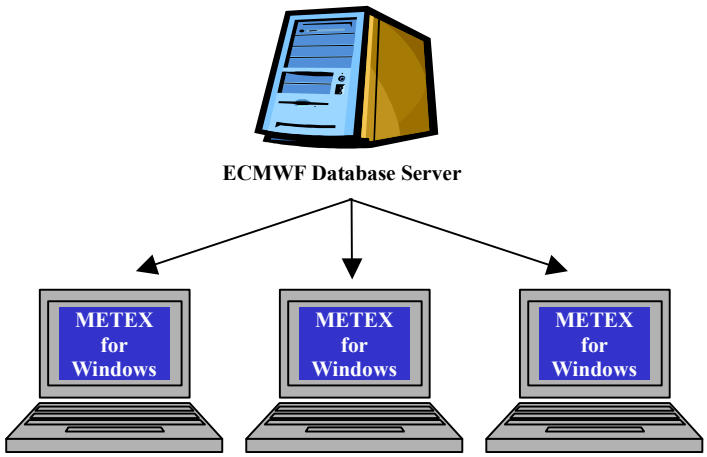

Figure 5 System configuration of METEX.

Table 1 Features of METEX and GMET.

	METEX	GMET
Language	C for user interface and all program components	User interface: C Numerical: Fortran Graphic: PV-Wave
Platform	PC with any version of 32-bit Windows (Windows 95®, 98®, ME®, NT4®, 2000®, and XP®)	Sun Workstation Ultra 10
Trajectory model	1) 3D-wind 2) Isentropic	1) Isobaric 2) Isentropic
Vertical coordinate	1) Absolute pressure 2) Terrain following hybrid sigma	Absolute pressure
Time step	Automatically adjust each time step according to wind velocity	Use a fixed time step for all trajectories of the same initialization conditions
Performance (3-day, hourly output)	30 lines per minute with 300 MHz CPU (180 lines per minutes with 1 GHz CPU)	One line per minute with 300 MHz CPU
Stability	Batch computing of trajectory for all available ECMWF data (1993 to 2002) without hang-up or memory leak	Stop in certain land-checking situations
Graphic format	PS, CGM, PDF, TIF, PNG, BMP, and real time display	PS, GIF, JPEG, TIFF, and real time display
Multi-access	Simultaneous use of the program by multi-users from their desktops is simple and easy	Simultaneous use might be OK, but requires the administrator to activate the remote access and users to know telnet or X-window for PC.
Data display	Wind field, pressure, and temperature of ECMWF data at given height	All ECMWF data at given pressure level; Time series change of a variable

2. ECMWF Dataset

2.1 Reprocessing Data

One of the distinguished characteristics of METEX is the computing speed, which is achieved partly by using re-processed meteorological data. As is described in the article of Zeng et al. (2003) for the encoding and decoding of ECMWF data, meteorological parameters in an ECMWF data file are stacked according to pressure levels and parameter ID (Figure 6). The number of parameter and pressure levels in CGER's ECMWF database varies from year to year.

Each record of a parameter includes five sections that contain variable amount information of GRIB encoding. The Indicator Section starts with the ASCII characters 'GRIB', indicating the beginning of a record. A decoding program can find the parameter ID in the Production Definition Section and find the decoding factors and the number of data in the Grid Description Section. The values of meteorological parameters are packed in two-byte integers in the Binary data section.

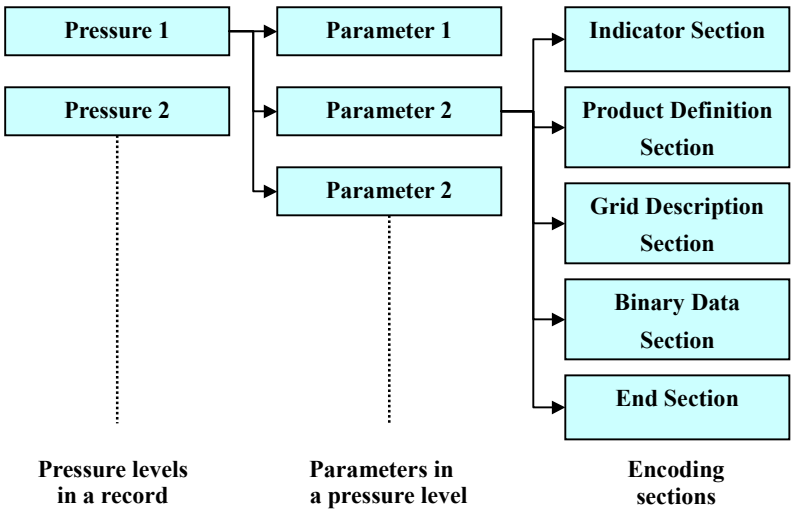

Figure 6 Internal layout of ECMWF data.

If the internal layout of ECMWF data files is as consistent as shown in Figure 6, reading parameters from a file could be efficient without reprocessing the data files. Unfortunately, the layout sequence of parameters for a given pressure level may change occasionally. The number of parameters on a pressure level also varies over the years. Thus the decoding routine of a trajectory programs (e.g., GMET) that use ECMWF's library may have to scan a file from beginning to end in order to obtain a parameter.

The first step we have taken in reprocessing ECMWF data was to make storage sequence of meteorological parameters exactly the same in all data files and to remove headers and parameters irrelevant to trajectory computing. A file of the new database contains only the geopotential, the *u*-, *v*-, and *w*-components of wind, and the temperature on all pressure levels (Figure 7). In contrast to variable file sizes that depend on the number of levels and parameters, the rearrangement results in fixed file sizes of 1.79 MB for 0.5-degree grid dataset on 15 pressure levels, 1.54 MB for 2.5 degree grid dataset on 15 pressure levels, and 83 KB for 2.5 degree grid dataset on the surface.

The conversion for surface data files is done separately because a different set of parameters is involved: the *w*-wind on the surface is zero and the surface pressure has to be included. Only one file containing the surface geopotential has been prepared for METEX, because this parameter is missing in the early ECMWF data files and because values of surface geopotential are expected to have small, if any, change.

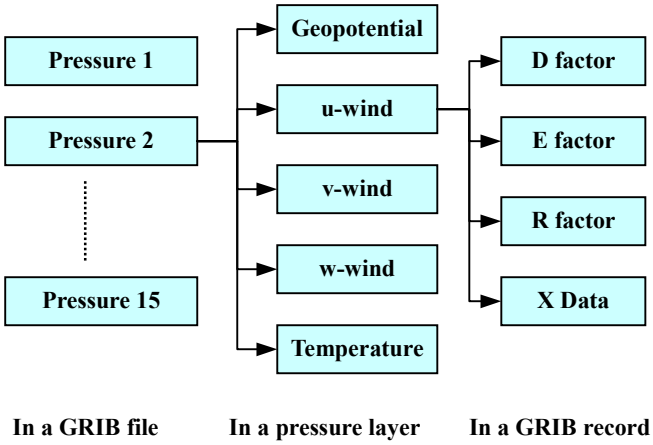

Figure 7 Structure of reprocessed ECMWF data.

On data input, METEX loads the reprocessed data in a lump sum and only decodes factors of D, E, and R, whose meanings are described by Zeng et al. (2003), for 5 parameters on 15 pressure levels. The binary data of X is decoded only for those 4 horizontal grids that enclose current trajectory position on 15 pressure levels. This scheme not only saves memory but also accelerates data manipulation immensely.

2.2 Database Structure

METEX uses three time-series datasets (0.5-degree grid and 2.5-degree grid on 15 pressure levels and 2.5-degree grid on the surface) and three single file datasets (etopo60.dat for terrain surface, geo25 for surface geopotential height, and map data for shorelines). The plain-file database structure is shown in Figure 8.

The surface geopotential of 2.5-degree grid is used for converting pressure coordinate to sigma coordinate. However, we use a 1×1-degree grid of topographic data in the output of trajectory so that we can detect trajectories that hit land more accurately from altitude output. The map data for graphic output come from the low-resolution dataset of the global shoreline database of Wessel and Smith (1996). We modified the dataset slightly to eliminate crossover lines that would otherwise occur in certain map projections.

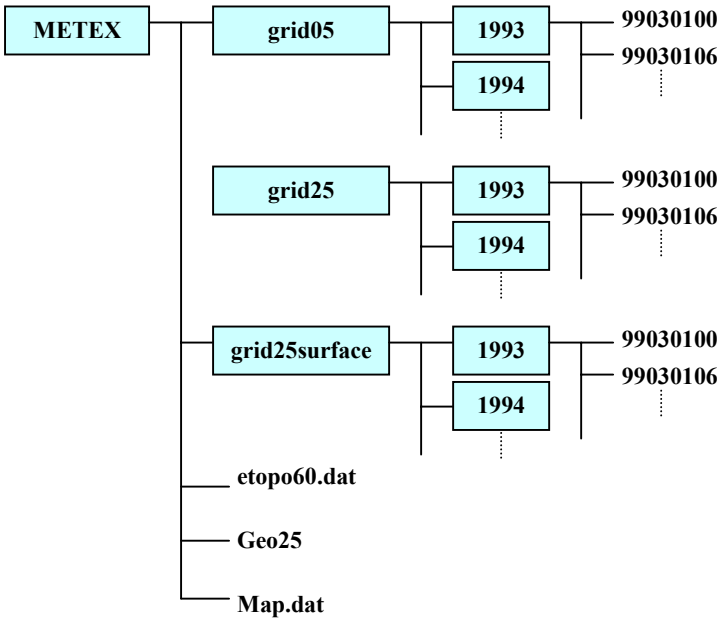

Figure 8 Database Structure of METEX

3. Trajectory Calculation Procedures

A trajectory calculation mainly involves spatial and time interpolation to obtain values of meteorological variable at a specific position and time from available data, and involves time integration to estimate the motion of an air parcel. The procedures are outlined as follows:

1). Initialize the program with latitude, longitude, altitude, and time.
2). Read and decode ECMWF data from files whose time intercept the initial time.
3). Find the grid box that enclose the given latitude, longitude, and altitude.
4). Calculate values of meteorological variables for the same latitude, longitude; and altitude for those times of the two ECMWF files by spatial interpolation using data on the eight corners of the grid boxes.
5). Calculate values of meteorological variables for the time and position of air parcel by time interpolation from the two spatially interpolated values.
6). Estimate the integration time step based on wind velocity.
7). Forward or backward the time by the integration time step.
8). Estimate the new position of the air parcel from wind variables by time integration.
9). Test whether data files need updating; if yes, go to the second step; if no, go to the third step.

3.1 Spatial Interpolation

In METEX, a variable in a grid box is first interpolated to the specified vertical position, which can be represented by geopotential height, potential temperature, pressure, or sigma; and then to the specified horizontal position. The procedure is reversed in GMET, that is that the interpolation is done horizontally and then vertically. The difference is illustrated in Figure 9.

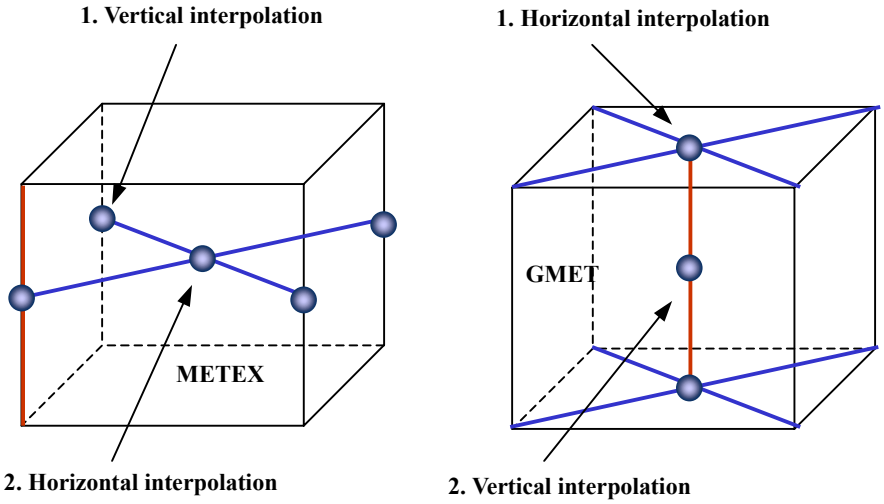

Figure 9 Spatial interpolations of METEX and GMET.

The basic assumption for vertical interpolation is that meteorological variables vary linearly with height, and therefore the value of a variable at a given height can be estimated by the closest two vertical points that intercept the height. Figure 10 is a plot of potential temperature versus geopotential height. One can see that the relationship between the two variables is composed of two linear sections jointed near the height of tropopause. The data in the figure comes from a grid near Hateruma station (24.05°N, 123.80°E) at 0:00 UTC on January 1, 2000. The potential temperature is calculated according to Draxler and Hess (1998) by

$$Q = T \cdot (1000 / P)^{0.286} \tag{1}$$

and the geopotential height by

$$H = \frac{G}{g} \tag{2}$$

where $g = 9.81$ m s^{-2} is the gravity acceleration constant.

Instead of height, it is more convenient to use pressure as the vertical coordinate in trajectory computing because parameters in the ECMWF dataset of CGER have been interpolated or extrapolated to constant pressure levels. According to the hydrostatic equation

$$\ln P = -\frac{g}{RT} Z \tag{3}$$

we expect that the logarithm of pressure P be nearly related to height. Results in Figure 11 shows that we can use ln$P$ interchangeably for height in the linear interpolation. Data in Figure 11 come from the same source of Figure 10. Here is the equation for vertical interpolation when the pressure coordinated is in use:

$$v = \frac{fp_k \cdot v_k + fp_{k+1} v_{k+1}}{fp} \tag{4}$$

where pressure interpolation factors are obtained by

$$\begin{aligned} fp_k &= \ln P - \ln P_{k+1} \\ fp_{k+1} &= \ln P_k - \ln P \\ fp &= \ln P_k - \ln P_{k+1} \end{aligned} \tag{5}$$

and the subscript k stands for the sequential number of pressure level counted from bottom up, and v the value of a parameter at pressure P that lies between P_k and P_{k+1}.

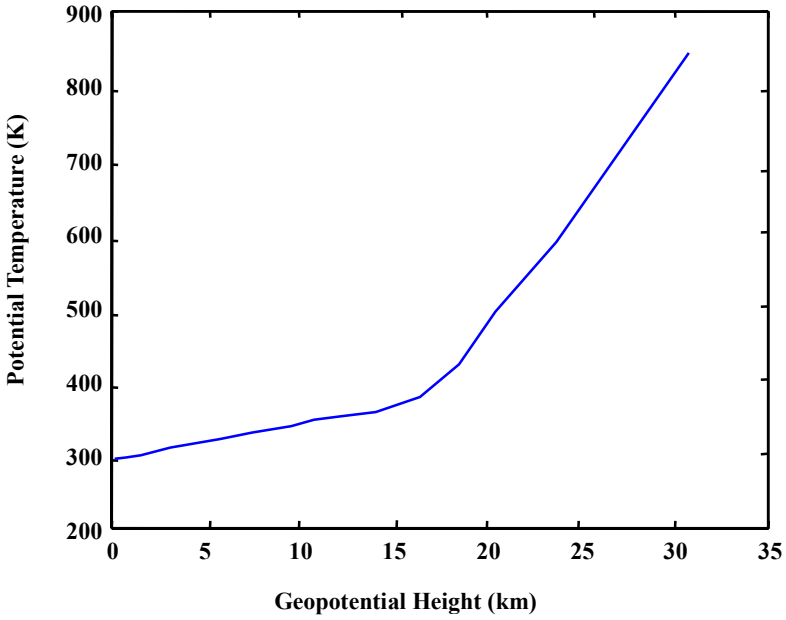

Figure 10 Relation between potential temperature and geopotential height.

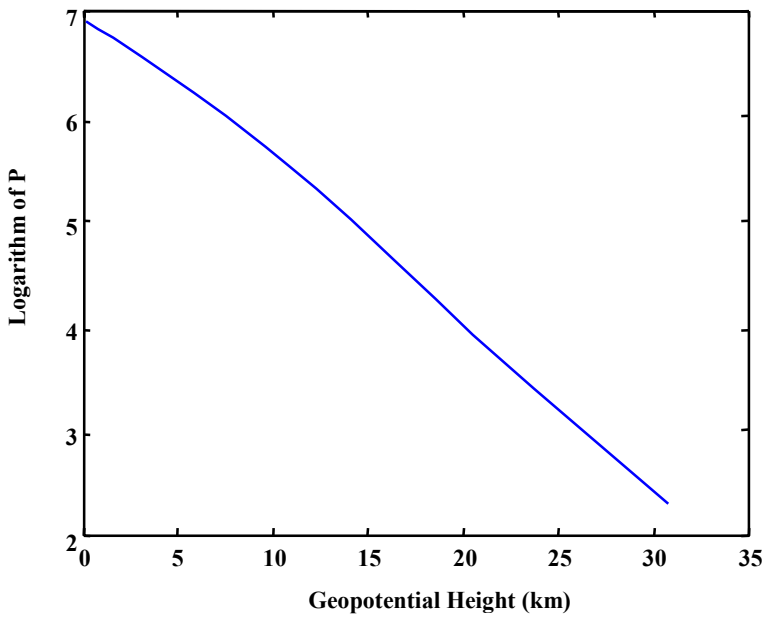

Figure 11 Relation between pressure and geopotential height.

3.2 Sigma Coordinate

In addition to the pressure coordinate used by GMET, METEX also implements the sigma coordinate for trajectory computing. There are two advantages by doing this: (1) land checking becomes unnecessary because of the terrain following characteristics of the sigma coordinate; and (2) comparison with other programs becomes easier because many programs implement only the sigma coordinate. HYSPLIT and FLEXTRA are two of such programs.

There are many ways to implement the sigma coordinate. For example, Draxler and Hess (1998) derived sigma from height while Haagenson et al. (1987) from pressure. METEX construct sigma from pressure, but in a different way from that of Haagenson et al. (1987).

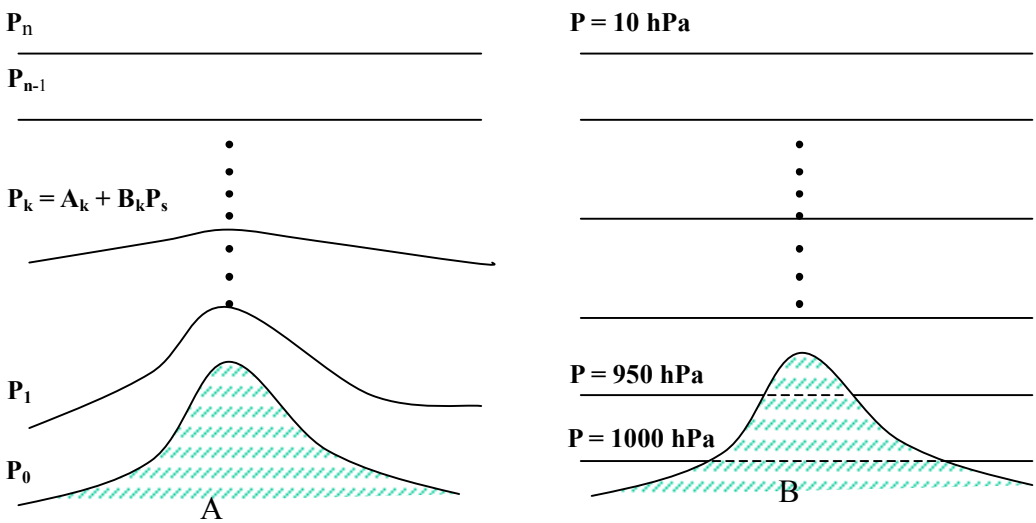

Figure 12 Hybrid vertical coordinate used by ECMWF's operational model (A) and absolute pressure coordinate of CGER's ECMWF dataset (B).

Before introducing METEX's sigma coordinate, we will explain briefly the hybrid vertical grid used by ECMWF's operational model and the absolute vertical pressure grid of CGER's ECMWF datasets (Figure 12). The hybrid coordinate of EMCWF is determined by:

$$P_k = A_k + B_k P_s \qquad (k = 0,1,...n) \tag{6}$$

where P_s is the surface pressure, and A_k and B_k are constants for pressure level k. P_n (k=n) equals to the pressure of the top pressure level in the absolute pressure coordinate. The values for A_k and B_k are listed in Table 2. We use the same set of values to determine the sigma levels of METEX except that the value of A_n is changed to 10 to make P_n inline with the value of the top pressure level. Considering the vertical interpolation requirement, we use the following function to calculate the sigma on level k:

$$\sigma_k = \frac{\ln P_k - \ln P_s}{\ln P_n - \ln P_s} \tag{7}$$

Obviously, the sigma varies from 0 to 1 with pressure from surface to the very top level. The interpolation equation (4) for sigma coordinate becomes:

$$v = \frac{fs_k \cdot v_k + fs_{k+1} v_{k+1}}{fs} \tag{8}$$

with

$$\begin{aligned} fs_k &= \sigma_{k+1} - \sigma \\ fs_{k+1} &= \sigma - \sigma_k \\ fs &= \sigma_{k+1} - \sigma_k \end{aligned} \tag{9}$$

Users may expect that the height output of trajectories be always positive when the sigma coordinate is used. However a negative number may occur in some areas where the surface geopotential of ECMWF data is smaller than zero.

Table 2 Parameters used to calculate the hybrid pressure levels from the surface pressure.

Level	A_k	B_k
19	0	0.0
18	20	0.0
17	40	0.0
16	60	0.0
15	83	0.004
14	106	0.014
13	128	0.035
12	146	0.072
11	158	0.127
10	161	0.202
9	153	0.296
8	136	0.405
7	111	0.524
6	82	0.645
5	52	0.759
4	26	0.856
3	8	0.929
2	0	0.973
1	0	0.992
0	0	1.0

3.3 Interpolation in 3D-Wind Model

The value of a meteorological variable $\Gamma(x,y,z,t)$ in a three dimensional space is obtained by linear interpolations for space (x,y,z) and time (t). In the 3D-wind model, $\Gamma(z)$ in a grid box (Figure 13A) is obtained by first calculating $\Gamma_i(z)$ for each grid using wind vectors on the two pressure or sigma levels whose vertical coordinates intercept the point and then calculating $\Gamma(z)$ by linear interpolation on the horizontal plane using the function:

$$\Gamma(z) = \frac{\sum_{i=1}^{4} fxy_i \cdot \Gamma_i(z)}{\sum_{i=1}^{4} fxy_i} \tag{10}$$

where horizontal interpolation factors are estimated from grid latitude x and latitude y (Figure 13B) by

$$\begin{aligned} dx_1 &= 1-(x-x_1)/(x_2-x_1) \\ dx_2 &= 1-(x_2-x)/(x_2-x_1) \\ dy_1 &= 1-(y-y_1)/(y_2-y_1) \\ dy_2 &= 1-(y_2-y)/(y_2-y_1) \\ fxy_1 &= dx_2 \cdot dy_2 \\ fxy_2 &= dx_1 \cdot dy_2 \\ fxy_3 &= dx_1 \cdot dy_1 \\ fxy_4 &= dx_2 \cdot dy_1 \end{aligned} \tag{11}$$

This method is equivalent to the two-step interpolation by latitude and longitude or vice versa. Note that in initializing the trajectory program, the vertical coordinate is the geopotential height; and the pressure, sigma, or potential temperature is the dependent variable. The relation is reversed in vertical interpolation for trajectory calculation.

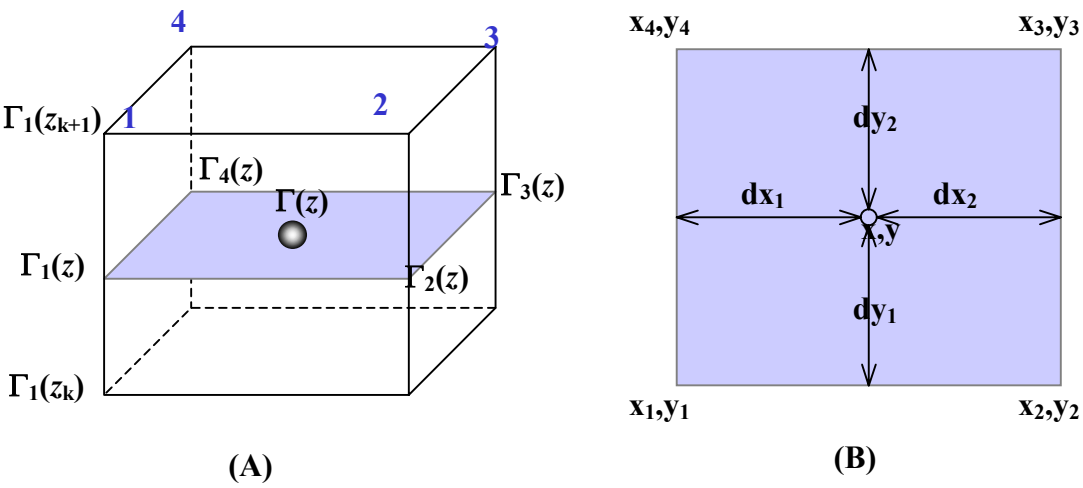

Figure 13 The spatial interpolation of the 3D-wind model for a grid box.

3.4 Interpolation in Isentropic Model

The horizontal interpolation for the isentropic model is slightly different from that of the 3D-wind model. Isentropic trajectories account for adiabatic vertical motions that air parcels may experience en route to their destinations. First of all, the first guess for the initial potential temperature Q_0 is done by the same interpolation procedures as those in the 3D-wind model for the initial pressure or sigma. We then iteratively re-evaluate the height at the given latitude and longitude by horizontal interpolation from heights of the four grid points on the isentropic surface (Figure 14) and by adjusting the potential temperature recursively until the height equals the starting altitude within a specified accuracy.

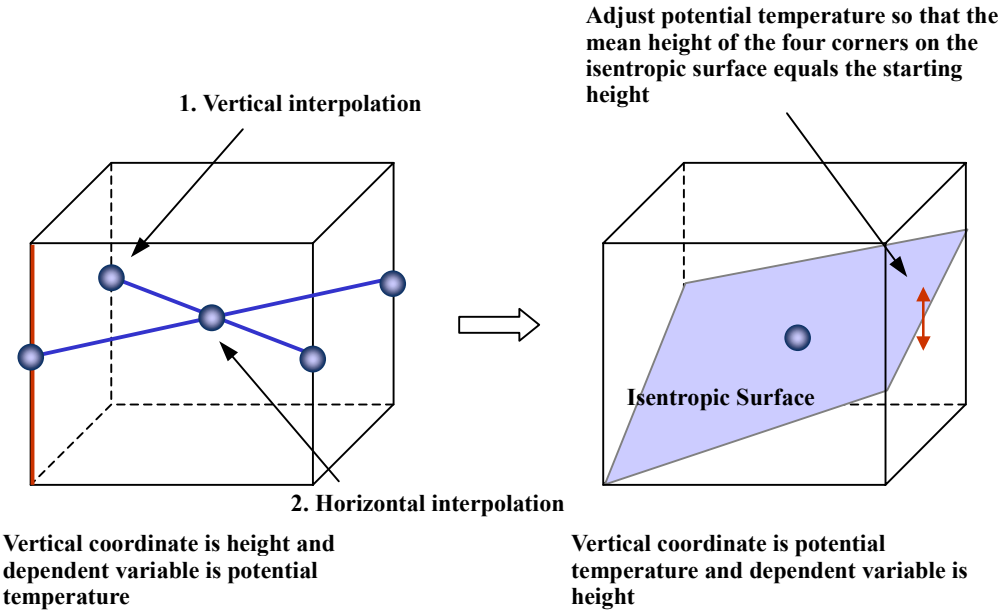

Figure 14 The spatial interpolation of the isentropic model.

After determined the initial potential temperature, we treat the isentropic surface as a flat plane and conduct horizontal interpolations for winds (u and v components only) in the same way as in the 3D-wind model. Whenever the current position moves to a different grid, we re-evaluated the isentropic surface and all relevant variables on the four grid points. We treat the isentropic surface simply as a flat plane because on true horizontal and vertical scales the isentropic surface in most grid boxes is nearly flat. For example, at latitude 30°N, the horizontal distance between two adjacent grids of 2.5 degree is about 240 km, whereas the distance between the first two pressure layers is about 0.7 km.

3.5 Time interpolation

The linear interpolation for time is similar to that of vertical interpolation, i.e.,

$$\lambda_t = ft_1 \cdot \lambda_1 + ft_2 \lambda_2 \tag{12}$$

and

$$ft_1 = \frac{|t_2 - t|}{|t_2 - t_1|}, \quad ft_2 = \frac{|t_1 - t|}{|t_2 - t_1|} \tag{13}$$

where the current time t is between the two data file time t_1 and t_2; and λ_1 and λ_2 are variables resulted from spatial interpolations at t_1 and t_2, respectively.

3.6 Time Integration

Both HYSPLIT and FLEXTRA programs use the method of Petterssen (1954) for the time integration. The UNIX version of GMET implemented methods of Euler, Petterssen, and the forth order Runge-Kutta. In theory, the accuracy of Petterssen method is higher than that of Euler but lower than that of the fourth order Runge-Kutta. Draxler and Hess (1998) investigated and rejected the fourth order Runge-Kutta method because, they concluded, that a higher order integration will not produce a better accuracy as long as observations are linearly interpolated from grids to the integration point. We adopted Petterssen's method for METEX.

According to Petterssen's method, a particle moving from position $L(t)$ to $L(t+\Delta t)$ is calculated by first estimating

$$L'(t + \Delta t) = L(t) + \Gamma(L, t) \cdot \Delta t \tag{14}$$

where $\Gamma(L,t)$ is the velocity vector; and then by

$$L(t + \Delta t) = L(t) + 0.5 \cdot \left[\Gamma(L, t) + \Gamma(L', t + \Delta t)\right] \cdot \Delta t \tag{15}$$

To achieve both good integration accuracy and fast computing speed, METEX adopted FLEXTRA's method of using flexible time steps in integration. The time step is determined according to the horizontal wind velocity by

$$\Delta t = \frac{\Delta D}{CFL \cdot \sqrt{u^2 + v^2}} \tag{16}$$

where ΔD is the distance between two adjacent horizontal grids and CFL stands for the Courant-Friedrichs-Lewy criterion. METEX uses the value 5 internally for CFL.

3.7 Conversion of Distance

The flexible time step method discussed previously guarantees that an air parcel will move no more than one fifth of a grid size in one integration step. This makes it safe to convert traveling distances along latitude and longitude from meter to degree by assuming a spherical earth when the air parcel is far from the North and South Poles, that is:

$$\begin{aligned} D2R &= \pi / 180 \\ R2D &= 180 / \pi \\ r_h &= r_e + h \\ r &= r_h \cdot \cos(D2R \cdot lat) \\ \Delta lon &= R2D \cdot \Delta x / r \\ \Delta lat &= R2D \cdot \Delta y / r_h \end{aligned} \tag{17}$$

where h is the height of air parcel at latitude lat and longitude lon and r_e the earth's radius.

In the Polar Regions, we approximate the spherical surface with a flat plane; and the conversion is done by converting the change of distance (Δx and Δy) in the Cartesian coordinates to the x-y position in the polar-stereographic coordinates (Figure 15) by

$$\begin{aligned} x &= r \cdot \cos(D2R \cdot lon) - \Delta x \cdot \sin(D2R \cdot lon) - \Delta y \cdot \cos(D2R \cdot lon) \\ y &= r \cdot \sin(D2R \cdot lon) + \Delta x \cdot \cos(D2R \cdot lon) \pm \Delta y \cdot \sin(D2R \cdot lon) \end{aligned} \tag{18}$$

where $\pm\Delta y$ is negative for the North Pole and positive for the South Pole. The x and y are then converted to longitude and latitude by

$$\begin{aligned} lat &= \frac{180}{\pi} \cdot \cos^{-1}\left(\frac{\sqrt{x^2 + y^2}}{r_h}\right) \\ lon &= \frac{180}{\pi} \cdot \tan^{-1}\left(\frac{y}{x}\right) \end{aligned} \tag{19}$$

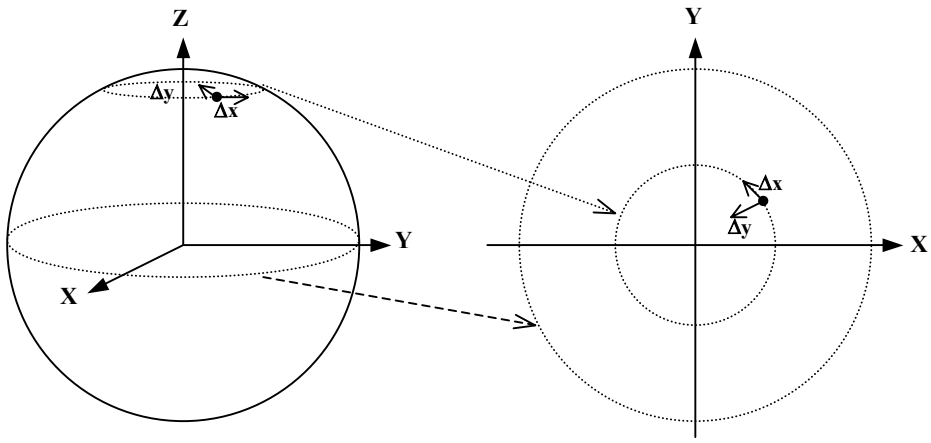

Figure 15 Illustration of coordinate conversion.

4. Land and Boundary Checking

4.1 3D-Wind Model

The land and boundary checking for the 3D-wind model is relatively simple. If the pressure coordinate is selected, METEX resets the pressure attribute of an air parcel to the pressure of the bottom layer when later is larger. The same method applies to the top pressure layer. The air parcel will never escape to outside the bottom layer in the sigma coordinate because the vertical wind on the surface is always zero. The air parcel may go beyond the top layer. This case is handled by METEX in the same way as in pressure coordinate.

4.2 Isentropic Model

There are four different cases of land and boundary checking that we have to deal with for the isentropic model, especially when the pressure coordinate is selected.

- When the air parcel moves to a high-pressure region, the first pressure level (P=1000 hPa) might be a few hundred meters above the sea surface. Some grids in the isentropic surface may lie below the lowest pressure level (Figure 16). In such a case, METEX resets the vertical coordinates of outlying grids to those on the first pressure level and add 100 to the output flag.

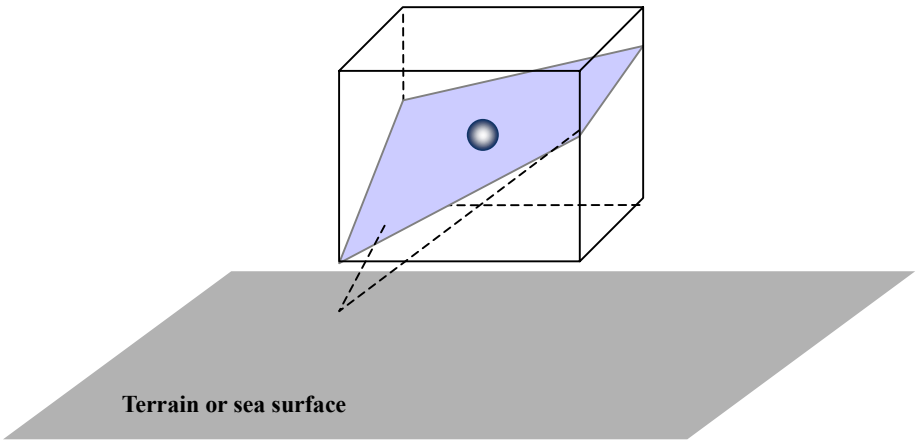

Figure 16 Case-1 of land and boundary checking.

- In some extreme situations (e.g., when the starting altitude is very high), some grids in the isentropic model may be above the top pressure level (Figure 17). In such a case, METEX reset the vertical coordinates of outlying grids to those of the top level and add 10000 to the output flag.

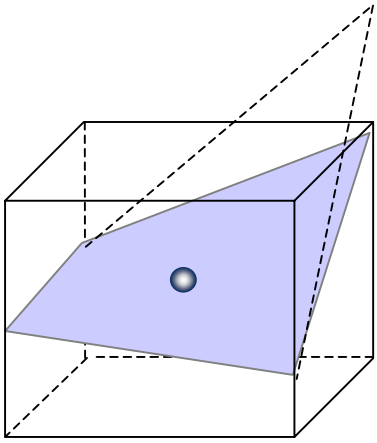

Figure 17 Case-2 of land and boundary checking.

- When the pressure coordinated is used and the air parcel is in a low-pressure region, the bottom plane of the grid box may lie under the ground (Figure 18). In

this case, we assume that meteorological variables on those virtual grids are valid and carry on spatial interpolation as usual. Such occasions are not flagged in the output. We believe the occurrence is rare and would not impose a larger effect on trajectory computing.

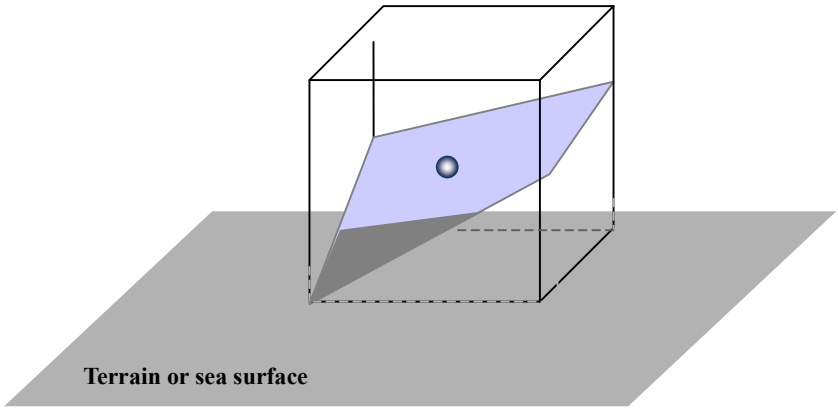

Figure 18 Case-3 of land and boundary checking.

- The last case we may encounter in using the pressure coordinate is when a pressure level intersects a mountain (Figure 19). For the same reason as in case 3, we assume that estimated wind vectors by including virtual grids are valid. You can identify such occasions by checking the output of terrain height.

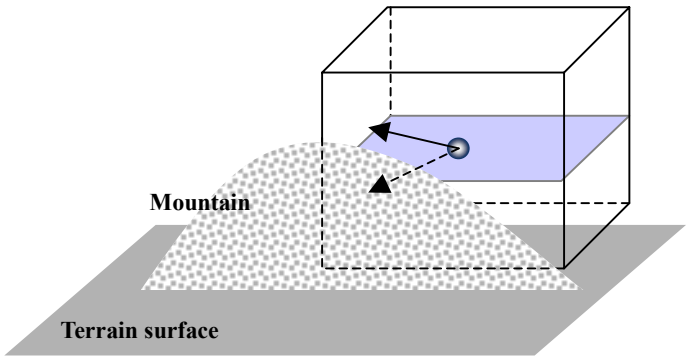

Figure 19 Case-4 of land and boundary checking.

4.3 Unstable Boundary Layers

The isentropic model has to deal with unstable boundary layers. Generally, the potential temperature increases with altitude, or decreases with pressure. If unstable boundary layers exist, a local minimum of potential temperature may occur. Figure 20 shows the variation of potential temperature with pressure at 43°N, 145°E on February 8, 2000, retrieved from the 2.5-degree grid database. The potential temperature on the layer P=925 hPa is smaller than

those on adjacent layers. If the initial potential temperature in a trajectory computing is larger than 284.0848 K and smaller than 284.0876 K, the isentropic model faces the dilemma of how to determine the altitude of the isentropic surface in this grid.

When the above situation occurs, METEX uses the altitude between the upper two layers. Because the unstable layer indicates the tendency of upward flow of air, setting the isentropic surface to the point between the upper two layers should give more realistic trajectory when the air parcel moves toward that grid. Whenever METEX encounters a grid having unstable layers, it adds one to the output flag so that the phenomenon can be easily identified.

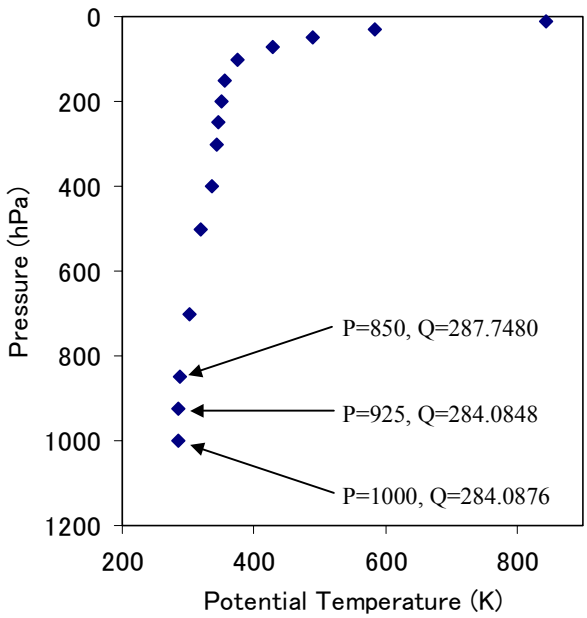

Figure 20 Variation of potential temperature with pressure at 43°N, 145°E, on February 8, 2000.

5. Verification and Comparison

5.1 Definition of Terms

Statistical terms used in discussions in this section are defined as follows and illustrated in Figure 21.

- An **Integrated Distance** D is the sum of distances between adjacent points along a trajectory, i.e.,

$$D = \sum d_{ij}$$

- The **Mean Integrated Distance** $\overline{D}$ is the mean of integrated distances of trajectories from two different programs or models of A and B, i.e.,

$$\overline{D} = \frac{1}{N}\sum_{i=1}^{N}\left(\frac{D_i^A + D_i^B}{2}\right)$$

Definitions for the minimum, maximum, and standard deviation of distance are parallel to that for the mean.

- A **Difference of Distance** ΔD is the distance between end-point pairs of two trajectories projected to the earth's surface.
- The **Mean Difference in Distance** $\overline{\Delta D}$ is the ratio of the mean of differences of distance between trajectories to the mean integrated distance, i.e.,

$$\overline{\Delta D} = \frac{1}{N}\sum_{i=1}^{N}\left(\frac{\Delta D_i^A + \Delta D_i^B}{2}\right) \Big/ \overline{D}$$

- A **Difference of Height** ΔZ is the vertical distance between endpoint pair of two trajectories projected to a plane perpendicular to the earth's surface, i.e.,

$$\Delta Z = \left|\frac{Z^A - Z^B}{2}\right|$$

- The **Mean Difference in Height** is the ratio of the mean of differences of height between trajectories to the difference of maximum and minimum of height difference, i.e.,

$$\overline{\Delta Z} = \frac{1}{N}\sum_{i=1}^{N}\Delta Z_i \Big/ (\Delta Z_{\max} - \Delta Z_{\min})$$

$$\Delta Z_{\min} = MIN(\Delta Z_i^{A,B}, i = 1 \rightarrow n)$$

$$\Delta Z_{\max} = MAX(\Delta Z_i^{A,B}, i = 1 \rightarrow n)$$

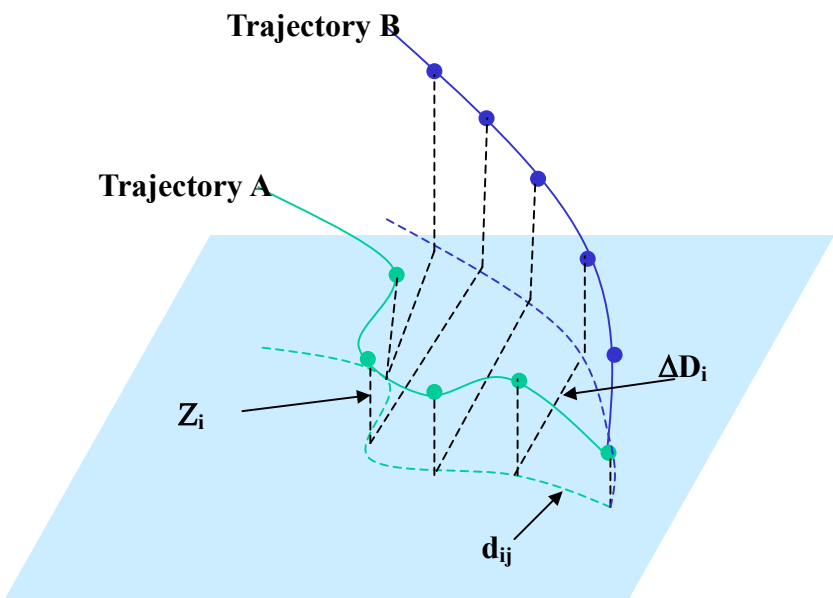

Figure 21 Illustration of parameter definition for trajectory comparison.

5.2 METEX vs. STRAS

The Stratosphere-Troposphere Research Assisting System (STRAS) is another trajectory program developed mainly for ozone monitoring research and Polar voltex forecast. The program includes both isentropic and 3D-wind models and can use either ECMWF or NCEP dataset.

We verified METEX by comparing its results with those of STRAS on the consideration that both programs use the same ECMWF dataset and can calculate trajectories with very similar initial conditions. The two programs are developed independently in different programming languages (METEX in C and STRAS in FORTRAN) for different platforms (METEX for PC Windows and STRAS for SUN UNIX Workstation). We have compared 3-day backward trajectories for Hateruma Station (Figure 22A) and the North Pole (Figure 22B) in 6-hour interval for year 2000, a total of 1,464 lines.

Trajectories from the two programs are laid out side by side for visual inspection. Trajectories from 3D-wind and isentropic models of STRAS are plotted in blue and yellow, and of METEX in green and red, respectively. Obviously, the same model of the two programs produces nearly identical results. The differences cannot be distinguished by color lines due to overlapping. However, trajectories from different models of the same program depart significantly in the end in the case of Hateruma, but the departure is much smaller in the case of the North Pole. This, of course, indicates the different natures of models, not the misbehaviors of programs.

Statistics from comparisons of the 3D-wind models of the two programs at Hateruma station are listed in Table 3, including a total number of 1397 lines, which is smaller than that in the visual comparison because not all trajectories are completely calculated for 72 hr by STRAS due to its land checking restrain.

The mean difference in distance shows that the two trajectory programs agree very well. Although, the mean integrated distance increase proportionally with time, the mean difference in distance varies only slightly from 0.15% to 0.17% with backward time from 24 hr to 72 hr. You may wonder why the mean difference in distance for 48 hr backward time is smaller than that for 24 hr backward time. The reason is that the difference is calculated from end points and not all pair of trajectories of METEX and STRAS astray farther apart with time – they may converge after a period of separation. The increase of the mean difference with time should become more obvious with increasing points of comparison.

Although the maximum difference in 72 hr is 26% of the mean integrated distance, differences exceeding 1% show only in 6 of all 1397 cases. The largest difference is caused by a short trajectory that passed though Taiwan Island. Different land checking methods of METEX and STRAS are the main cause of this large difference.

The relative difference in height between trajectories of METEX and STRAS is several times smaller than that in distance, as suggested by the mean difference in height. Even the maximum difference in height is less than 1% of the height variation range.

The integration method of STRAS is the fourth order Runge-Kutta, different from the Petterssen's method of METEX. The comparison has approved the conclusion of Draxler and Hess (1998) that high order of integration method is unnecessary, especially when proper times steps are used.

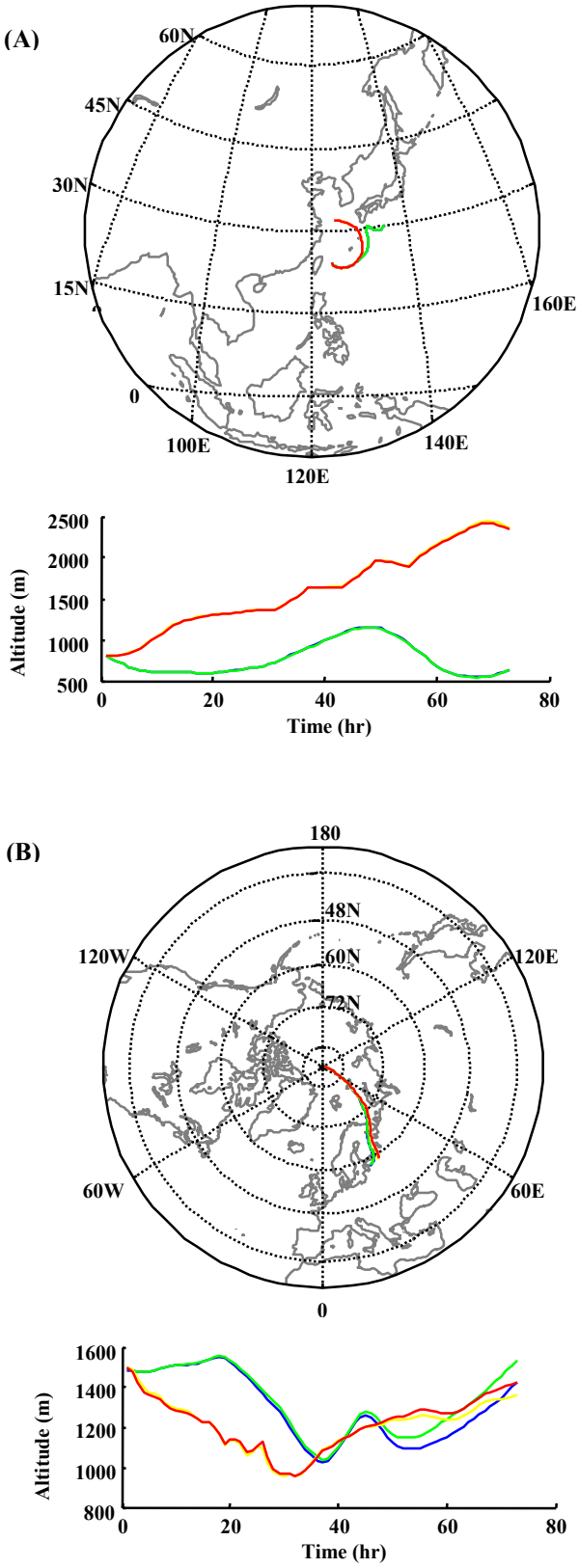

Figure 22 A visual comparison of METEX with STRAS: (A) Hateruma Station at 12:00 UTC on January 4, 2000; (B) North Pole at 6:00 UTC on January 5, 2000. Blue: STRAS-3D; Green: METEX-3D; Yellow: STRAS-IS; Red: METEX-IS.

Table 3 Statistics of comparisons between 3D-wind models of METEX and STRAS using trajectories at Hateruma station in 2000 with starting altitude of 800 m.

Backward Time	24 Hours	48 Hours	72 Hours
Mean Integrated Distance (km)	639	1287	1981
Minimum (km)	102	307	517
Maximum (km)	1801	3239	5452
Standard Deviation (km)	291	581	918
Mean Difference in Distance (%)	0.15	0.14	0.17
Minimum (%)	0.00	0.00	0.00
Maximum (%)	1.29	6.86	26.34
Standard Deviation (%)	0.14	0.21	0.72
Mean Altitude (m)	976	1424	1900
Minimum (m)	129	118	46
Maximum (m)	2585	5723	8153
Standard Deviation (m)	405	937	1402
Mean Difference in Height (%)	0.04	0.03	0.05
Minimum (%)	0.00	0.00	0.00
Maximum (%)	0.31	0.93	0.91
Standard Deviation (%)	0.04	0.05	0.07

5.3 METEX vs. GMET

We used 3-day backward trajectories at the Hateruma station in 2000 for comparing METEX with GMET. The starting altitude is 800 m and the interval between trajectories is 12 hr. Three time integration (Euler, Petterssen, and 4th order Runge-Kutta) and two spatial interpolation (grid linear and reversed distance) methods were implemented by GMET (Katsumoto et al., 2002). Unfortunately, the Petterssen's method in GMET was bound to the reversed distance interpolation method that had a problem in calculating wind vector near grid borders. Therefore we used the combination of linear interpolation and the 4th Runge-Kutta integration of GMET in trajectory calculation. Figure 23 is an example of visual comparisons between results from isentropic models of METEX and GMET.

Table 4 summarizes statistics of the comparison. Here the mean integrated distance and the mean altitude vary in similar magnitudes to those in Table 3. However, the mean differences in distance and height between METEX and GMET are large, about 12% and 3% respectively. In a severe case, as is implied by the maximum difference of distance, the separation between trajectory end points of METEX and GMET after 72 hr of backward time can be as large as the mean integrated distance. Similar to results in Table 3, the mean difference in height is several times smaller than the mean difference in distance.

Table 4 Statistics of comparisons between isentropic models of METEX and GMET using trajectories at Hateruma station in 2000 with starting altitude of 800 m.

Backward Time	24 Hours	48 Hours	72 Hours
Mean Integrated Distance (km)	568	1153	1786
Minimum (km)	85	300	492
Maximum (km)	1739	3814	5085
Standard Deviation (km)	267	550	862
Mean Difference in Distance (%)	13	11	12
Minimum (%)	0	0	0
Maximum (%)	75	71	99
Standard Deviation (%)	11	10	12
Mean Altitude (m)	1165	1454	1734
Minimum (m)	203	176	197
Maximum (m)	2912	5154	6196
Standard Deviation (m)	479	880	1235
Mean Difference in Height (%)	2	2	3
Minimum (%)	0	0	0
Maximum (%)	21	54	60
Standard Deviation (%)	3	4	5

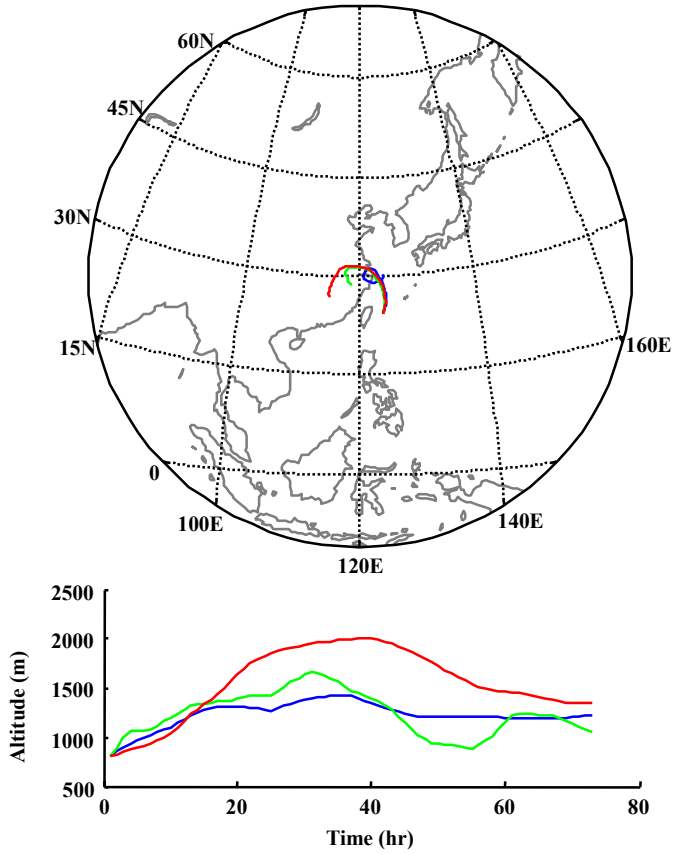

Figure 23 Trajectories from the isentropic (green) and 3D-wind (red) models of METEX and from the isentropic model of GMET. Blue: GMET-IS; Green: METEX-IS; Red: METEX-3D.

Because it has been approved by Draxler and Hess (1998) and by the comparisons between METEX and STRAS that the difference of trajectory caused by different integration methods is insignificant, the differences between isentropic models of METEX and GMET should be mainly caused by methods of interpolation and procedures of determining the isentropic surface. For the spatial interpolation of METEX in a grid box, a variable is first interpolated to the specified vertical position (can be represented by geopotential height, potential temperature, pressure, or sigma), and then to the specified horizontal position. The procedure is reversed in GMET, that is that the interpolation is done horizontally and then vertically.

GMET also estimates the initial potential temperature differently from that by METEX and STRAS. After the horizontal interpolation, GMET searches for potential temperature along the vertical coordinate represented by geopotential height. After that, re-evaluation for the height of the isentropic surface is not necessary for GMET, but essential for METEX and STRAS. Therefore the resulting potential temperatures for the same starting altitude may differ significantly.

However, even if we adjust METEX's initial potential temperature to the same value as that of GMET in a trajectory computing, we expect that the resulting compensation to the difference be limited because the vertical position change of an air parcel caused by the adjustment would not exceed 100 m and, as will be shown in the comparison for starting altitude, the difference caused by such a change in altitude is only about 5%.

5.4 Sigma vs. Pressure

One of the advantages of METEX over GMET is that trajectories can be calculated in a sigma coordinate system. The terrain following characteristics of sigma coordinate eliminated the problem of land checking so that an air parcel is guaranteed to move above the terrain surface. Here we provide some basic statistics on comparisons of trajectories obtained by using pressure and sigma coordinates. Again, we use results for Hateruma in 2000 with starting altitude of 800 m. We leave comparisons between models in the next discussion and only use the 3D-wind model here.

The differences introduced by different coordinate systems are about 5% for distance and 3% for height (Table 5). The former is about half of the difference introduced by isentropic models that implement different interpolation methods (Table 3). The minimum difference of altitude for 24 hr backward time is negative, indicating that some trajectories descended to the 1000 hPa pressure layer in low-pressure regions. Although no further comparison has been done, we believe that the difference will be smaller for oceanic areas, but larger in areas having more complicated topographic surroundings.

Table 5 Statistics of comparisons between sigma and pressure coordinates of METEX using trajectories at Hateruma station in 2000 with starting altitude of 800 m.

Backward Time	24 Hours	48 Hours	72 Hours
Mean Integrated Distance (km)	624	1267	1972
Minimum (km)	102	278	524
Maximum (km)	1790	3439	5664
Standard Deviation (km)	289	583	943
Mean Difference in Distance (%)	4	4	5
Minimum (%)	0	0	0
Maximum (%)	24	49	86
Standard Deviation (%)	3	4	6
Mean Altitude (m)	932	1376	1886
Minimum (m)	-16	10	28
Maximum (m)	2563	6084	8276
Standard Deviation (m)	413	1011	1531
Mean Difference in Height (%)	2	2	3
Minimum (%)	0	0	0
Maximum (%)	13	22	38
Standard Deviation (%)	2	4	5

5.5 Isentropic vs. 3D-Wind

In addition to the sigma coordinate, another new feature of METEX in comparison with GMET is the 3D-wind trajectory model. Comparisons between the two models are scarce in literature. In the report of Haagenson et al. (1987), the prediction by isentropic model agreed with observations slightly better than other models, including the 3D-wind model. However, the vertical motion in their work was calculated using data from the Cross Appalachian Trace Experiment (CAPTEX' 83), not from observation or long-range forecast modeling. The inter-comparison by Kahl et al. (1989) indicates large discrepancies between isentropic and 3D-wind models. Because different programs were involved, it is difficult to evaluate exactly how much difference the two models can produce. We discuss this issue here using METEX's results.

Based on trajectory results at Hateruma station, we observed that the mean difference in distance between the isentropic and the 3D-wind model (Table 6 and Table 7) is twice as large as that caused by difference interpolation methods (Table 4) and four to five time larger than that caused by difference vertical coordinates (Table 5). The comparisons for pressure (Table 6) and sigma (Table 7) coordinates shows small differences between statistical parameters of the two coordinate except for the minimum difference in distance. The reason for the exception is that the air parcel is confined within the range of 1000 hPa to 10 hPa in the pressure coordinates, but within the range of surface pressure to 10 hPa in the sigma coordinate. The mean difference in distance increases with the mean integrated distance or backward time consistently.

The difference between results of the two coordinates depends greatly on the surrounding area where trajectories are calculated. A direct support for the argument can be found in the statistics in Table 8, which summarizes comparisons between 3D-wind and isentropic models for 25°N, 160°E with similar initial conditions as those for Hateruma station. With the starting position moved farther away from the Asian continent, the mean difference in distance decrease by half (see Table 6 and Table 8), even though the mean integrated distance increases by perceptible amount; and the mean difference in height also decreases slightly. Indirect supports for the argument can be found in visual comparisons between trajectories at the North Pole and Hateruma station (Figure 22) and a visual comparison along ship routes of M/S Skaugran in the North Pacific (Figure 24).

Further, Figure 25 clearly shows patterns that relate the mean difference in distance to the horizontal position of end points for Hateruma station. Here the differences of distance is categorized by three colors: (1) green for those smaller than 1000 km, (2) blue for those between 1000 km and 2000 km, and (3) red for those larger than 2000 km. Most of the differences fall in the first category, indicating that the difference does not fit to the normal distribution. Larger differences occur more likely in trajectories originated in the north or the northwest of the station. The difference seems related to the characteristics of heat fluxes of land and ocean to a great extent if the spatial gradient of potential temperature is considered. At Hateruma station the gradient at the same height is characteristically larger toward the north (Figure 26).

All comparisons in this section are for finding out differences between the two models. Further studies are necessary to evaluate their trajectory quality. However, a noticeable phenomenon for the isentropic model is that the air motion is most likely upward when a backward trajectory goes toward the north of Hateruma. The distribution of potential temperature has determined such a trend, which in our opinion may be a bias. Katsumoto et al. (2002) have discussed the phenomenon in more details in a case study.

Table 6 Statistics of comparisons between 3D-wind and isentropic models of METEX using trajectories at Hateruma station in 2000 with starting altitude of 800 m. The vertical coordinate is pressure.

Backward Time	24 Hours	48 Hours	72 Hours
Mean Integrated Distance (km)	595	1207	1867
Minimum (km)	104	310	550
Maximum (km)	1762	3534	5379
Standard Deviation (km)	275	548	853
Mean difference in Distance (%)	21	25	27
Minimum (%)	0	0	0
Maximum (%)	153	117	172
Standard Deviation (%)	23	26	28
Mean Altitude (m)	1047	1396	1756
Minimum (m)	59	85	93
Maximum (m)	2826	5495	7015
Standard Deviation (m)	418	882	1246
Mean difference in Height (%)	12	9	10
Minimum (%)	0	0	0
Maximum (%)	55	65	73
Standard Deviation (%)	10	8	10

Table 7 Statistics of comparisons between 3D-wind and isentropic models of METEX using trajectories at Hateruma station in 2000 with starting altitude of 800 m. The vertical coordinate is sigma.

Backward Time	24 Hours	48 Hours	72 Hours
Mean Integrated Distance (km)	580	1187	1858
Minimum (km)	104	281	549
Maximum (km)	1736	3734	5570
Standard Deviation (km)	270	547	880
Mean difference in Distance (%)	20	24	28
Minimum (%)	0	0	0
Maximum (%)	183	190	184
Standard Deviation (%)	24	27	29
Mean Altitude (m)	1040	1411	1823
Minimum (m)	-1	6	2
Maximum (m)	2792	5913	7161
Standard Deviation (m)	411	946	1369
Mean difference in Height (%)	12	8	11
Minimum (%)	0	0	0
Maximum (%)	57	55	82
Standard Deviation (%)	11	7	11

Table 8 Statistics of comparisons between 3D-wind and isentropic models of METEX using trajectories at 25°N, 160°E in 2000 with starting altitude of 800 m. The vertical coordinate is pressure.

Backward Time	24 Hours	48 Hours	72 Hours
Mean Integrated Distance (km)	593	1285	2016
Minimum (km)	131	289	448
Maximum (km)	1877	4405	6832
Standard Deviation (km)	277	655	1106
Mean difference in Distance (%)	8	11	14
Minimum (%)	0	0	0
Maximum (%)	92	116	110
Standard Deviation (%)	10	14	17
Mean Altitude (m)	1008	1358	1739
Minimum (m)	144	130	125
Maximum (m)	3342	6432	7355
Standard Deviation (m)	400	944	1394
Mean difference in Height (%)	8	7	9
Minimum (%)	0	0	0
Maximum (%)	64	84	90
Standard Deviation (%)	8	8	11

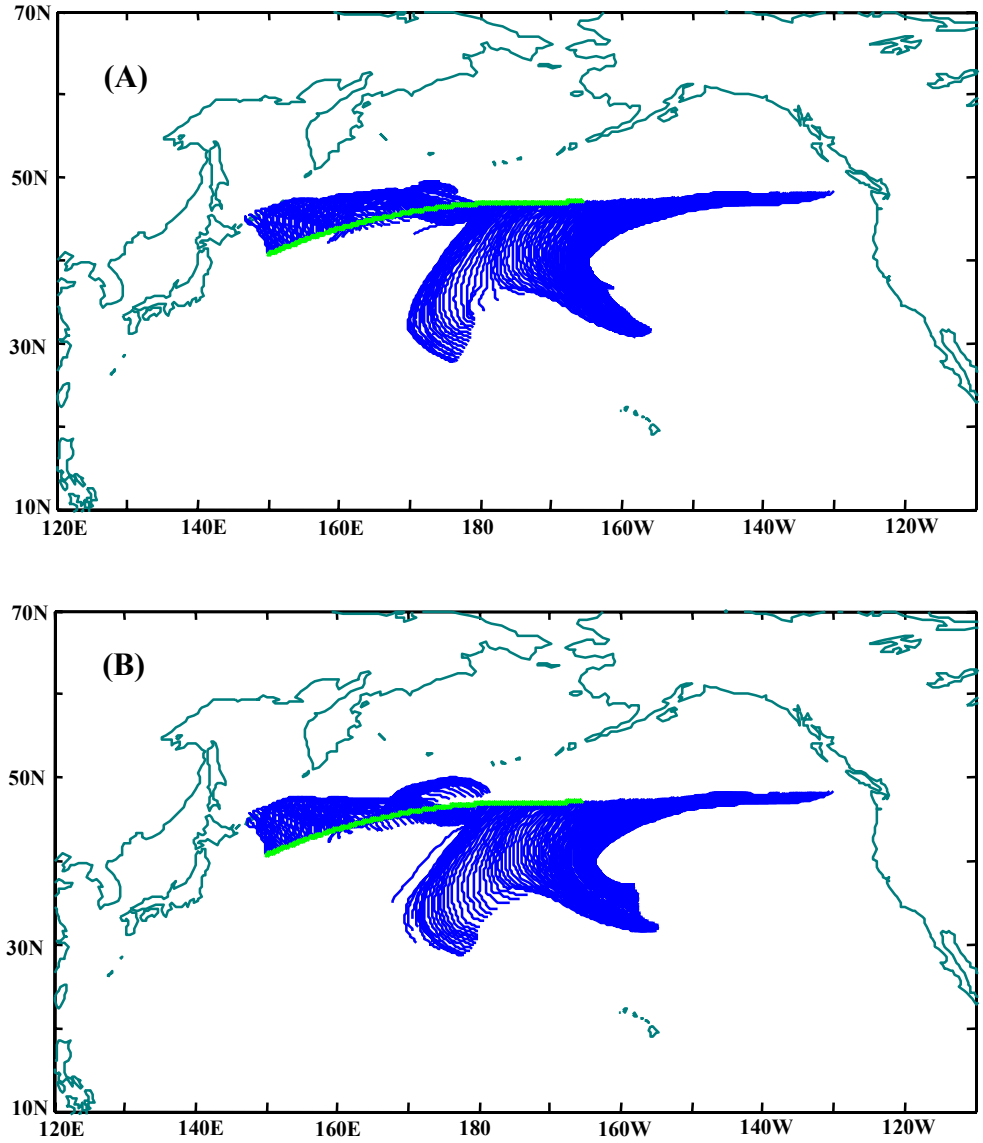

Figure 24 Comparison of trajectories between the 3D-wind model (A) and the isentropic model (B) for the ship route of M/S Skaugran in August 3, 1995 to August 13, 1995. Each plot has 250 trajectory lines.

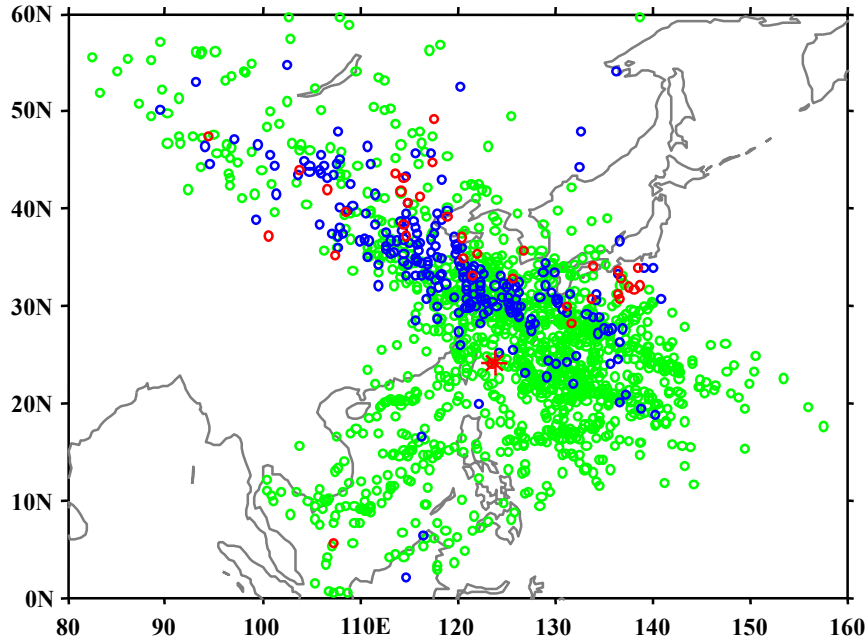

Figure 25 Distribution of the mean difference for Hateruma station; (1) green: $\overline{\Delta D} \leq$ 1000 km; (2) blue: 1000 km < $\overline{\Delta D}$ <2000 km; and (3) red: $\overline{\Delta D}$ ≥ 2000 km.

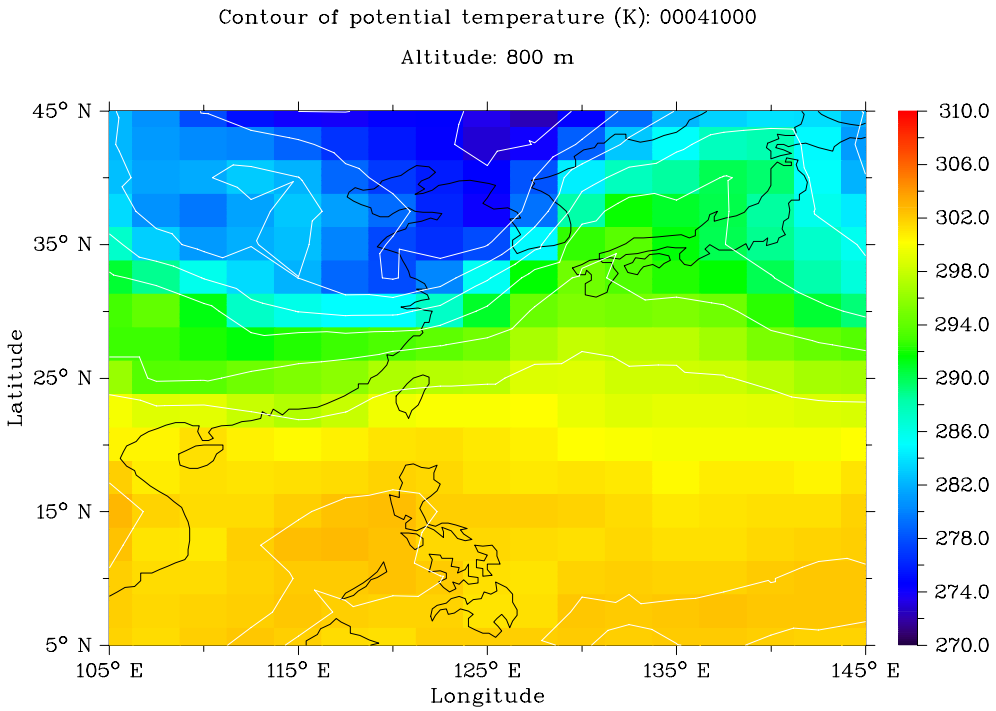

Figure 26 Distribution of potential temperature around Hateruma station at 800 m, 0:00 UTC April 4, 2000.

5.6 Starting Altitudes

Another question concerning the application of trajectories to atmospheric observations is how to select the starting altitude. Previous comparisons are conducted exclusively for the starting geopotential height of 800 m because it was a standard option for GMET in the past in the consideration that the height is near the second pressure level of ECMWF database and was not considered too low to lead the trajectories hitting the ground quickly or to cause pre-mature stop of a computing. With the introduction of sigma coordinate in METEX, trajectory computing can be initiated at any height above the surface. Some literatures suggest not using the surface wind field (e.g., Haagenson et al., 1987), but a high starting altitude alone may result in a large deviation of air motion from the surface because of the Ekman spiral phenomenon.

We used one year's trajectories at eight starting altitudes of 200 m, 400 m, 600 m, 800 m, 1000 m, 1200 m, 1400 m, and 1600 m in the investigation for altitude effect. The model is 3D-wind; and the targets include Hateruma station and the location of 25°N, 160°E. Roughly, altitudes lower than 800 m lie between the first two pressure levels (1000 hPa and 925 hPa) and those higher than 800 m between the second and the third pressure levels (925 hPa and 850 hPa).

The mean difference in distance between different starting altitudes is surprisingly large (Table 9), increasing linearly with the gap between starting altitudes. On average, a difference of 100 m in starting altitude induces a difference of 4.6% of the mean integrated distance at Hateruma station (Table 10). It is common to find that starting altitudes chosen in different researches differ by a few hundred meters. Assuming that altitudes of 500 m and 1000 m are selected by two independent studies for the same location, resulting trajectories could deviate by about 23%. Therefore, differences caused by starting altitudes are as serious as by trajectory models (Table 6).

The mean difference in distance between starting altitudes decreases significantly with the location change from Hateruma station to 25°N, 160°E, where the difference is about 3.4% per 100 m or 17% per 500 m on average (Table 10). However, the decrease in the difference is not as larger as in comparisons between isentropic and 3D-wind models for difference starting locations. Further studies are necessary to know what starting altitude is appropriate for a given location.

Table 9 Relative deviations of trajectories between different starting altitudes; location: 24.05°N, 123.8°E; period: January 2000 to December 2000, 6-hour interval; model: 3D-wind; vertical coordinate: Sigma; backward time: 72 hours; and number of points: 1,464.

Unit: %	400 m	600 m	800 m	1000m	1200m	1400m	1600m
200 m	11	22	31	40	47	55	64
400 m		13	24	33	42	51	59
600 m			13	24	34	44	54
800 m				13	25	36	47
1000 m					14	27	39
1200 m						15	29
1400 m							16

Table 10 Relative deviations between different starting altitudes; location: 25°N, 160°E; period: January 2000 to December 2000, 6-hour interval; model: 3D-wind; vertical coordinate: sigma; backward time: 72 hours; and number of points: 1,464.

Unit: %	400 m	600 m	800 m	1000m	1200m	1400m	1600m
200 m	9	18	24	31	36	42	47
400 m		9	17	24	31	36	42
600 m			9	17	24	31	37
800 m				9	17	25	31
1000 m					9	17	25
1200 m						9	17
1400 m							9

5.7 Summary

Comparisons discussed so far are only part of the tremendous amount of tests we carried out for diagnosing all options and the functioning of METEX. The program is very fast and stable. System hang-up or premature abortion of computing has never occur to the released versions in any lengthy computing, e.g., continuous trajectory computing for a 8-year period of 6-hour interval.

We have verified the numerical methods of METEX by comparing with STRAS. Although the two programs were developed independently in different programming languages for different platforms, no significant difference was detected in trajectory outputs.

Under the same initializing condition, trajectories vary to different extents according to the length of backward or forward time, location, trajectory models, starting altitudes, method of spatial interpolation, and types of vertical coordinates. Various comparisons suggest that it is imperative to carry out further studies to determine proper selections of initial condition in trajectory computing, especially the trajectory model and starting altitude. Differences caused by these two factors are much larger than those by others. The comparisons with GMET indicate that implementing different spatial interpolation methods induces a much larger effect on trajectory results than implementing various time integration methods. However, the resulted differences are small comparing with the differences caused by trajectory models and starting altitude. The least severe factor is the selection of pressure and sigma coordinates. An obvious advantage of the sigma coordinate is that trajectories will not move into a virtual space as may occur in pressure coordinate.

6. Supporting Data Analysis

6.1 CO_2 Time Series

We have produced animations for Hateruma station using 3-day backward trajectories and observed CO_2. Please refer to Mukai et al. (2001) for details of CO_2 monitoring at the station. The animation proves to be an effective media to examine the time series change of CO_2 with the origin of air parcels.

Figure 27 shows two snap shots of the animation for 2000. The CO_2 plot includes 30-days' observations of 6-hourly means from hourly data. The 3-day backward trajectory in Figure 27A indicates that the relatively high CO_2 at 6:00 UTC on January 19, 2000 (marked by the red dot) may be caused mainly by the source of air coming from the main land of China; meanwhile Figure 27B shows that the trajectory path in the last several hours has critical effect on CO_2 concentration. In this case the air also passed through China, but the CO_2 was low because the air went a long way through the oceanic area before reaching the destination. Figure 28 present two more examples supporting the argument, in which local minimum and maximum CO_2 occurred within 12 hours from 12:00 on February 19 to 0:00 on February 20, 2000; and the high CO_2 is related to a trajectory passed through Taiwan Island a few hours before the observation time, but the low CO_2 to a trajectory stayed on the east side of Taiwan Island.

Examining CO_2 change through trajectories is effective for Hateruma station in boreal winder when the north-south gradient of CO_2 is large and the terrestrial sink of CO_2 is near zero in the northern hemisphere (Conway and Tans, 1999). The examination becomes complicated in summer because a region of strong industrial CO_2 source may also be a comparatively strong terrestrial CO_2 sink.

The above examinations will become more complicated when the altitude of trajectories is considered. An air parcel directly coming from high CO_2 regions to the observation location may not raise the CO_2 value significantly when the air parcel is descended from high altitudes. However, simply referring to trajectory altitude is not sufficient because what appears high above the sea level on a flat map may be actually close to the terrain surface (Figure 29). Fortunately, METEX exports topographic height along with the trajectory height, allowing users to investigate the details.

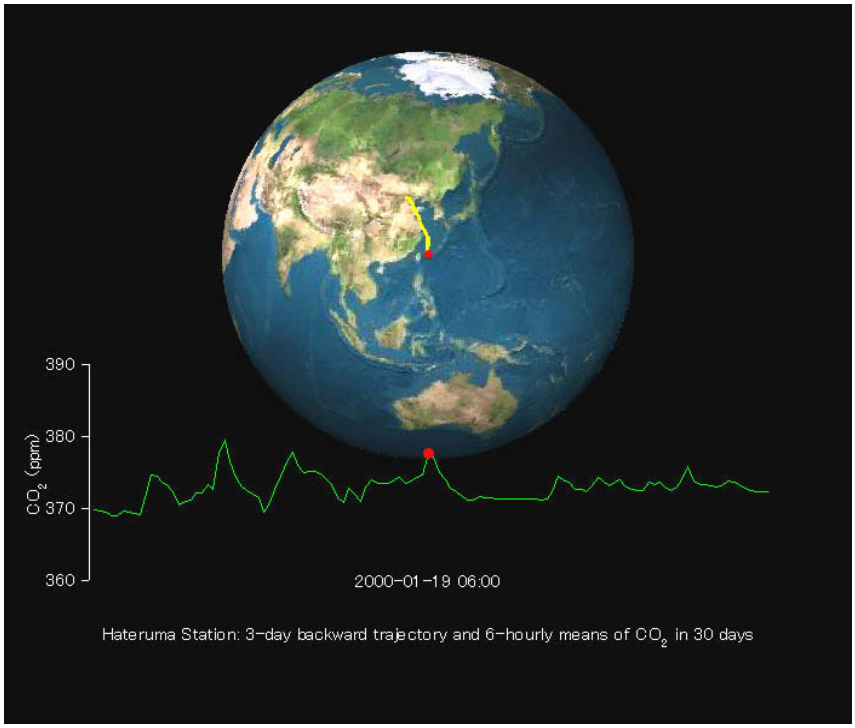

(A)

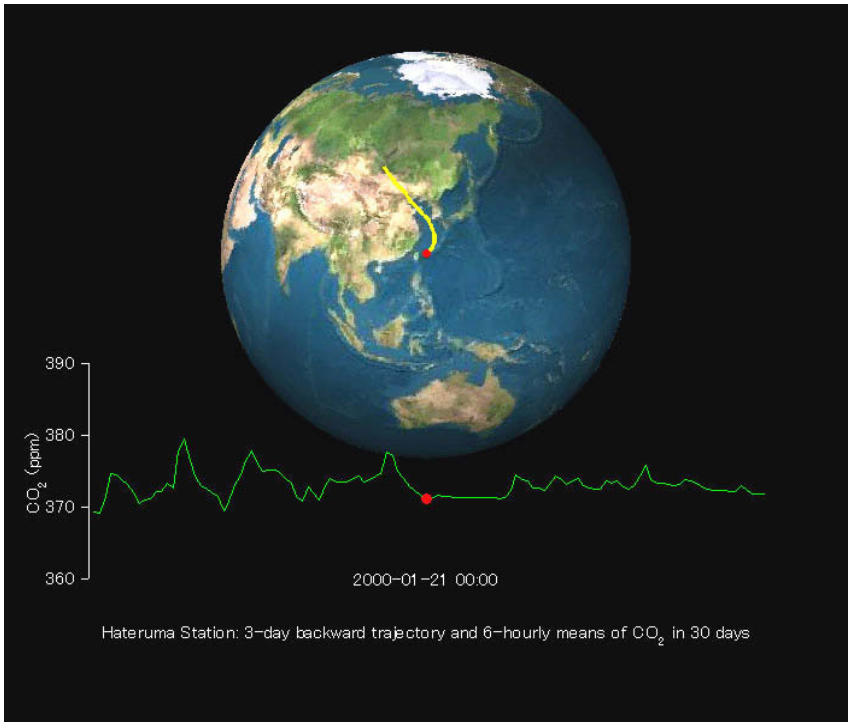

(B)

Figure 27 Snap shots of animations of trajectories and CO_2 time series at Hateruma station. The CO_2 plot contains 30-days' observations of 6-hourly means of hourly data. The red dot marks the CO_2 value at the displayed date and time. The corresponding 3-day backward trajectory is drawn on the globe with a red dot indicating the station's position.

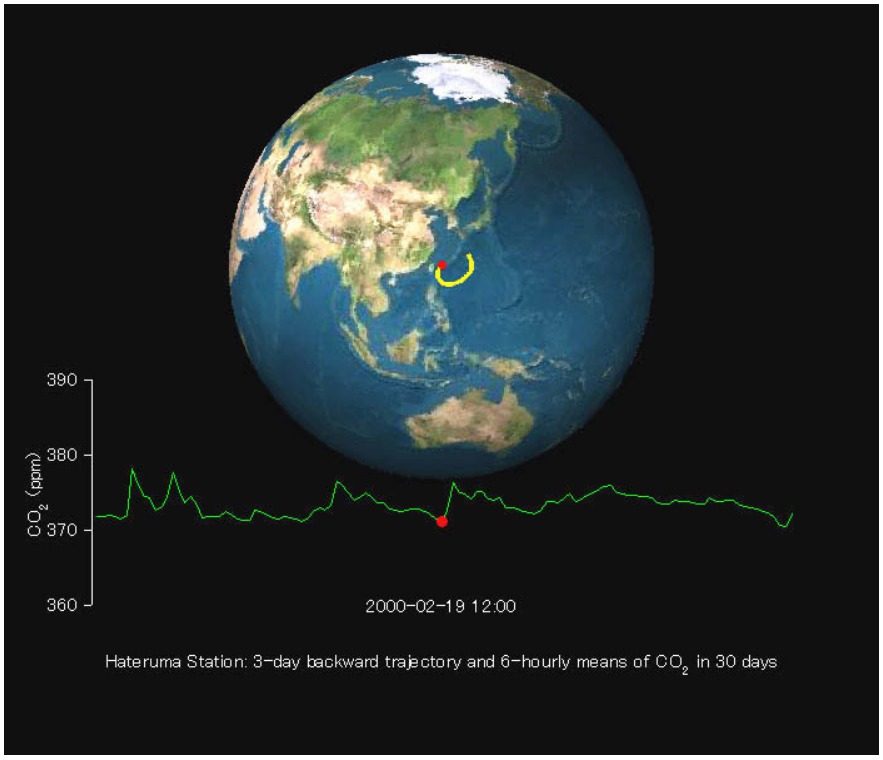

(A)

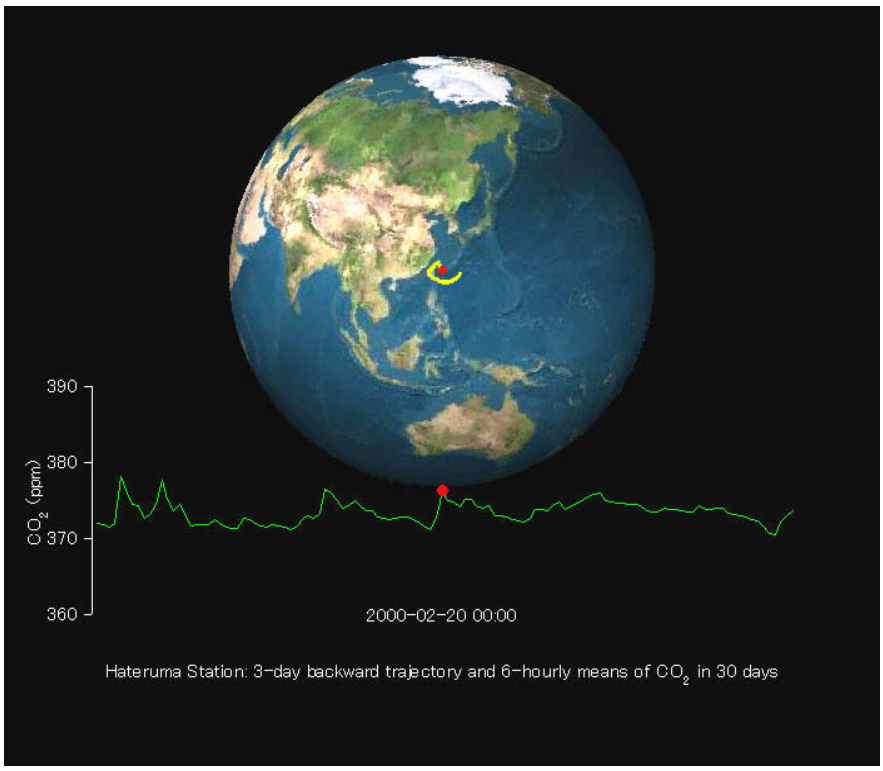

(B)

Figure 28 Snap shots from animations for trajectories and CO_2 time series of Hateruma station. These plots show that the air mass passed through Taiwan Island had caused a increase of atmospheric CO_2.

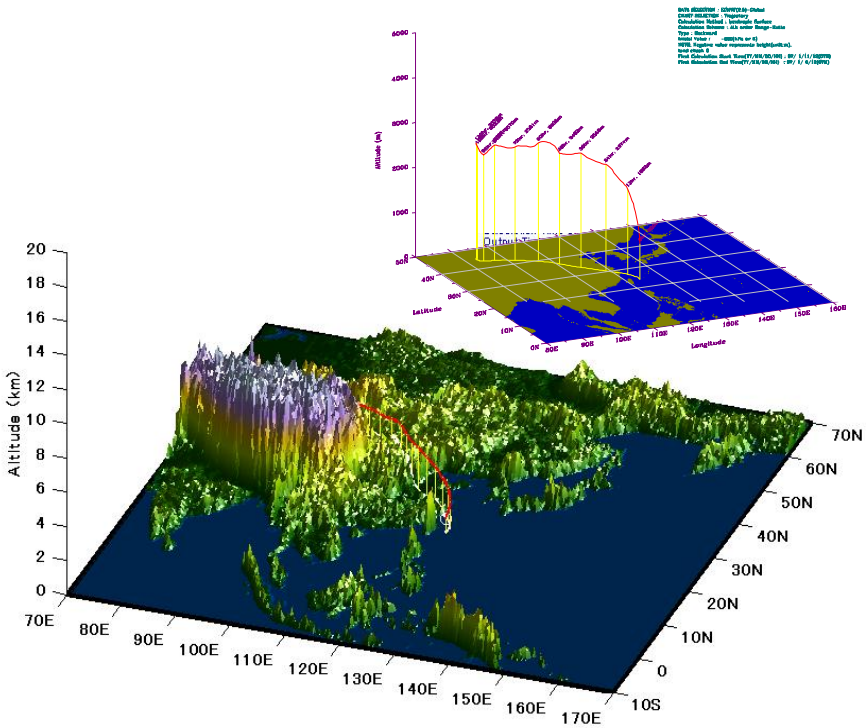

Figure 29 Three-dimensional plots of a trajectory.

6.2 Spatial CO_2 Variations

In contrast to a fixed station, applying trajectories to examine CO_2 changes observed by research vessels involves both time and spatial factors. Not being able to repeat the observation for the same location increases the complexity of analysis. Here we will present some results from analyzing CO_2 data obtained by M/S Skaugran, a commercial cargo ship used by the ship-of-opportunity project of the National Institute for Environmental Studies, Japan, and the Institute of Ocean Sciences, Canada (Nojiri et al., 1999; Murphy et al., 2001). The dataset contains atmospheric and oceanic CO_2 in 1995 to 1999 in the North Pacific. The ship routes are shown in Figure 30. The time series data were detrended (removing the anthropogenic increase) to permit comparison of CO_2 observed in different years. Daily means of CO_2 at Heteruma, Cape Ochiishi, Minamitorishima, and Mauna Loa were used to estimate the long-term trends of CO_2. Detrended CO_2 at these stations along with those at Shemya Island, Sand Island, Cold Bay, and Cape Meares, where CO_2 sampling intervals are irregular, were used to model seasonal changes surrounding the North Pacific. Data of Hateruma and Ochiishi were described by Mukai et al. (2001); data for Minamitorishima are provided by Japan Meteorological Agency and were described by Otomo et al. (2000); and data at the rest of stations are provided by U.S. National Oceanographic and Atmospheric Administration/Climate Monitoring and Diagnostics Laboratory and were described by Conway et al. (1994). All data came from The World Data Center for Greenhouse Gases and The Carbon Dioxide Information Analysis Center.

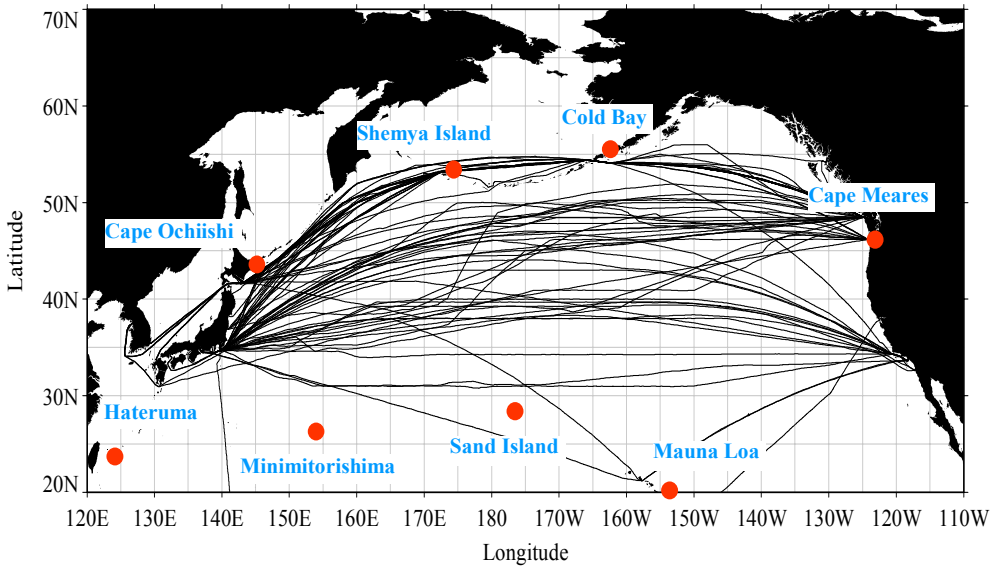

Figure 30 Routes of M/S Skaugran and fixed stations used to detrend CO_2 obtained by the ship.

Following the work of Thoning et al. (1989), we obtained trends using FFT with a cutoff frequency of 0.5 for the exponential low-pass filter. Changes of CO_2 with time were made approximately stationary by subtracting the trend determined by the first and the last points. A stationary time series was augmented with the first year of data at the beginning and the last year of data at the end to reduce the end effect of aliasing. The benchmark trend of CO_2 was selected based on comparisons of long-term trends among stations. We subtracted the benchmark trend from each time series and then fitted the detrended time-series data using the following equation:

$$f(t) = a + \sum_{k}^{3} [b_k \sin(\frac{2\pi kt}{365}) + c_k \cos(\frac{2\pi kt}{365})] \tag{20}$$

Where t has the unit of day. Data from multiple years were overlapped to produce a single set of coefficients for estimating the seasonal change.

Estimating CO_2 at a given time and position in the area surrounded by fixed stations was done by interpolation. Since observation stations are scattered around the North Pacific unevenly and the longitudinal gradient of CO_2 is generally smaller than the latitudinal gradient, we interpolated based on latitude and distance using the following function:

$$C_{cal} = \left(\sum_{i=1}^{n} (1 - \frac{|L - L_i|}{DL}) \cdot e^{-k \cdot d_i / DM} \cdot C_i \right) \Big/ \left(\sum_{i=1}^{n} (1 - \frac{|L - L_i|}{DL}) \cdot e^{-k \cdot d_i / DM} \right) \tag{21}$$

Where n is the number of stations, L the latitude, DL the latitude scale factor, k the exponential parameter, d_i distances between ship's positions and station positions, DM the distance scale factor, and C_i the CO_2 at each station. The interpolation function is constructed so that (1) calculated CO_2 is close to fixed station CO_2 when the distance is zero and (2) At a given longitude CO_2 varies with latitude linearly. DL is set to the latitude difference between Minamitorishima and Cold Bay. DM is set to the distance between Minimatorishima and Cape

Meares. Parameter k is set to 7 so that the effect on calculated CO_2 by the most remote station is less than 0.1%.

Results in Figure 31 are a comparison of observed CO_2 (green circles) with modeled CO_2 (blue crosses) and trajectory corrected CO_2 (red triangle) in March 1997, a total of 181 points. A trajectory correction for modeled CO_2 was done by calculating CO_2 using equation (21) for positions of hourly output of 3-day backward trajectories and then calculating the mean as the corrected CO_2. The trajectories were obtained using the 3D wind model.

The latitude change of the ship course is small for this crossing, whereas the range of CO_2 variation is about 6 ppm, about twice as large as the north-south gradient of 3.3 ppm between Shemya and Sand Island in the same season. The trajectories show that air masses east and west of 175°W were originated from different regions. Modeled CO_2 with trajectory correction agrees with the observed CO_2 much better than those without correction. What appeared initially as an east-west gradient of CO_2 distribution was actually caused by the north-south gradient through atmospheric transport.

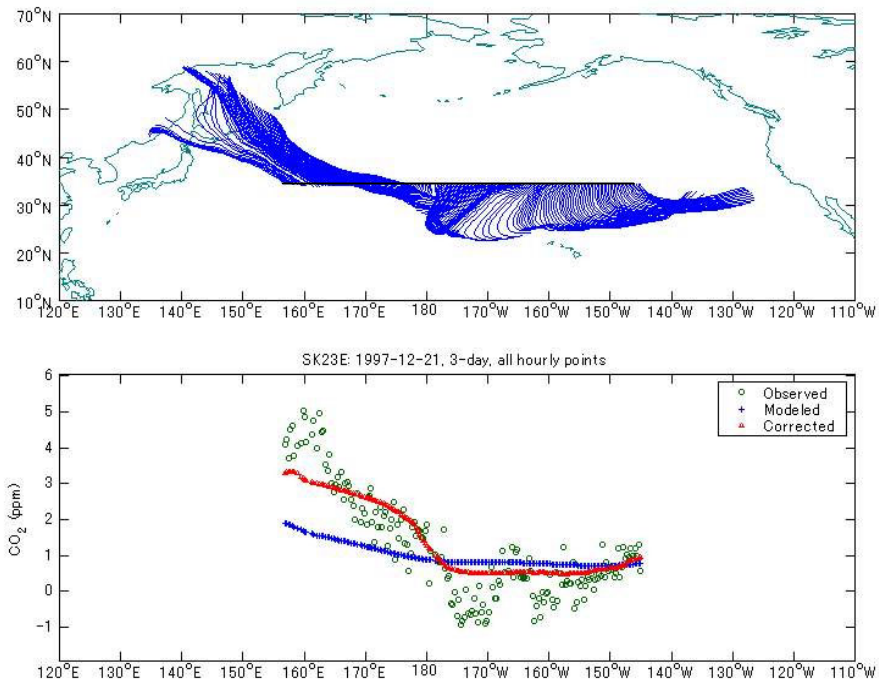

Figure 31 Comparison of observed CO_2 (green circle) in March 1997 with modeled CO_2 (blues cross) and trajectory corrected CO_2 (red triangle).

6.3 Seasonal CO_2 Variations

A comparison for the seasonal CO_2 variation observed by M/S Skaugran in the area of 40°N-45°N and 145°E-150°E is shown in Figure 32. After being fitted to equation (20), the multiple years of data exhibit a remarkable seasonal change similar to that observed at Ochiishi station (43.15°N, 145.5°E). Two observations in the August of 1998 and 1999 depart from the fitted curve severely. By examining the trajectories of those two crossings, we found a reasonable explanation that the high CO_2 observed in 1998 were caused by airs south of Ochiishi, whereas the low CO_2 in 1999 were caused airs from the northern-west Pacific, north of Ochiishi. The difference of the two observations is closed to that between Shemya and Sand in the same month.

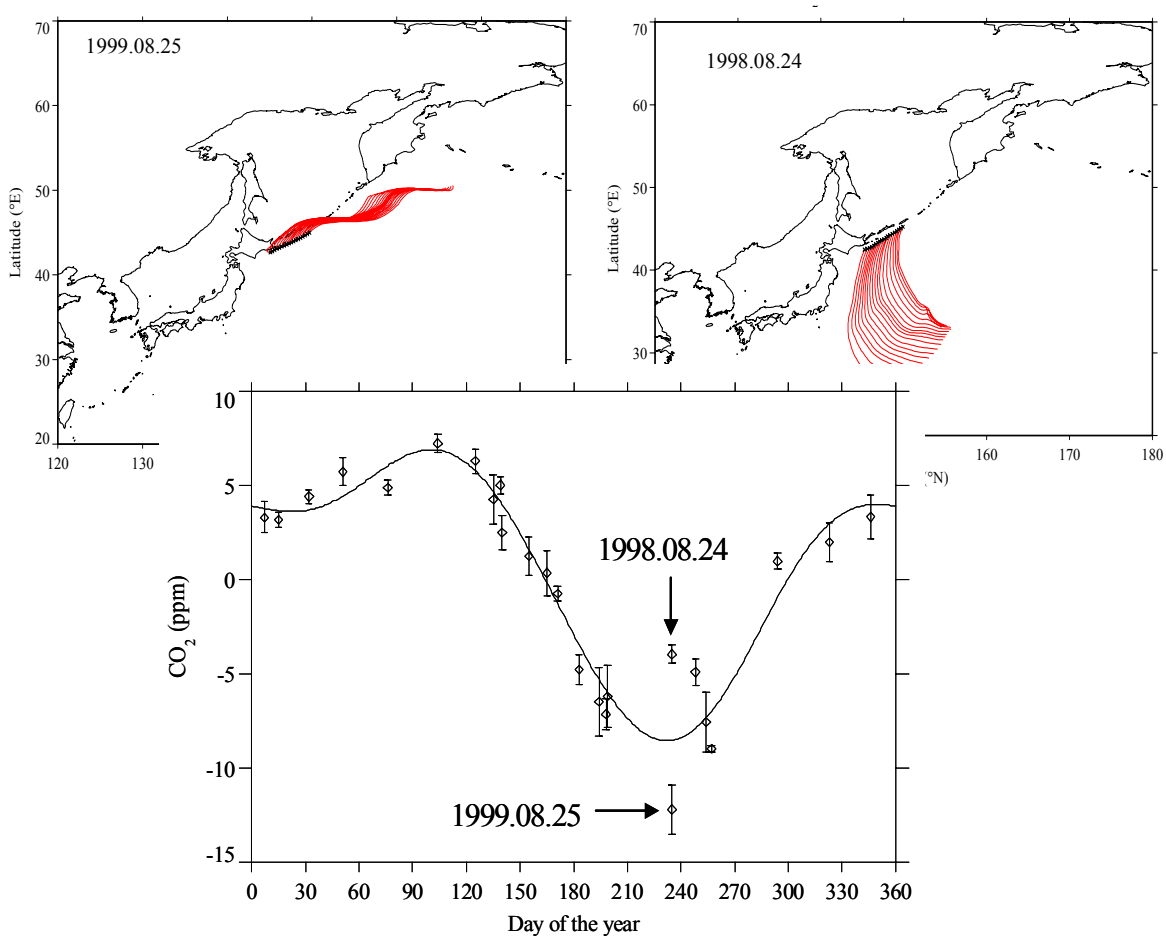

Figure 32 Examining seasonal CO_2 variations through trajectories.

7. Instructions for Building METEX

7.1 Conventions

The following two terms are defined to simplify discussions on the structure and development of METEX system:

- A MODULE consists of several subroutines in a C source file to perform a certain sort of functions;
- A COMPONENT consists of one or more modules and can be compiled to form an independent program that can be used to accomplish specific tasks;

METEX consists of four components (Figure 33): the graphic user interface (GUI), the data conversion tool (DCT), the graphic view tool for ECMWF parameters (GVT), and the trajectory tool (TRT). The DCT, GVT, and TRT components are written in ANSCII C and can be compiled as independent console programs by supplying a main function. Subroutines in the GUI component are strongly bounded to the 32-bits Windows API and designed for passing user inputs to other components. Therefore, compilation of METEX depends on whether you want to have the GUI in your program. The function calls between modules are shown in Figure 34.

The author has developed METEX using LCC-Win32 (http://www.cs.virginia.edu/~lcc-win32/), a free compiler system for Windows by Jacob Navia. No third party library is used except the freeware version of DISLIN (http://www.linmpi.mpg.de/dislin/) for LCC-Win32. Those who prefer to compile METEX from source code and to have graphic output must download the DISLIN library by themselves.

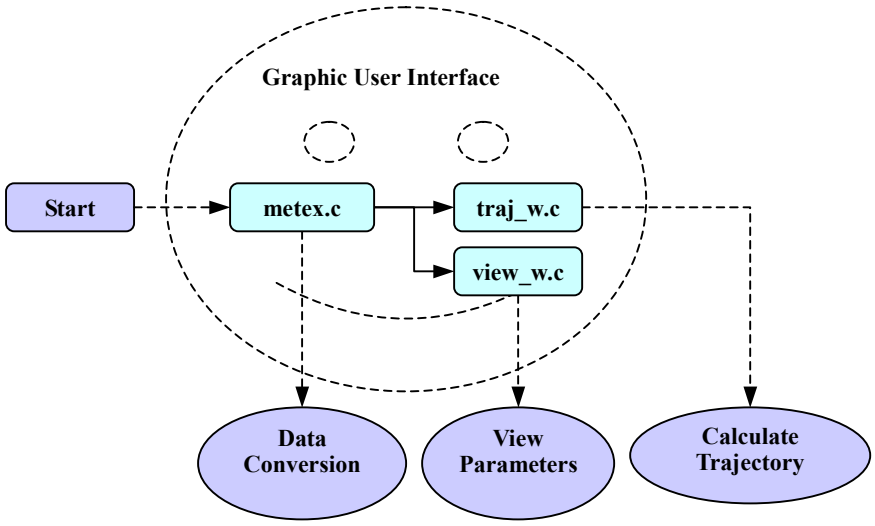

Figure 33 Structure of METEX system.

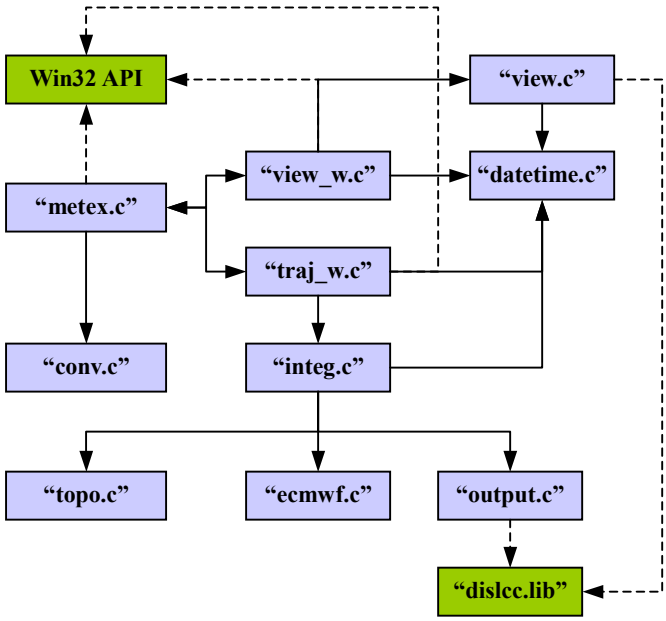

Figure 34 Function calls between modules.

7.2 GUI Component

The GUI component consists of three modules (Figure 33). The dynamic link library (DLL) of DCT is statically linked to the main window module (source file "metex.c"). The DLLs of GVT and TRT will be loaded at run time by corresponding modules (in "view_.c" and "traj_w.c"). Compiling the GUI needs knowledge about the Windows operation systems and compilers that can handle Windows resource file. Windows API references can be downloaded from Microsoft's website (http://www.microsoft.com/msdownload/platformsdk/sdkupdate/). Since the GUI only calls Win32 API functions, you don't have to use Microssoft's Visual C++ to accomplish the compilation. Besides LCC-Win32 system, you can use the free C and C++ compiler from Borland (http://community.borland.com/) for the job. In addition to those relevant files in Appendix B, the following image files are also required to compile the GUI:

"globe0.ico" --- icons for animation to signal the running status of METEX
"globe1.ico"
"globe2.ico"
"globe3.ico"
"globe4.ico"
"globe5.ico"
"globe6.ico"
"globe7.ico"
"globe8.ico"
"traj.ico" --- METX program icon
"metex.bmp" --- METEX image
"run.bmp" --- image for "run" tool button

“traj.bmp” --- image for “trajectory” tool button
“view.bmp” --- image for “view” tool button

The GUI component involves modules of “metex.c”, “conv.c”, “view_w.c”, and “traj_w.c”. Function calls in these modules are illustrated in Figure 35 to Figure 38.

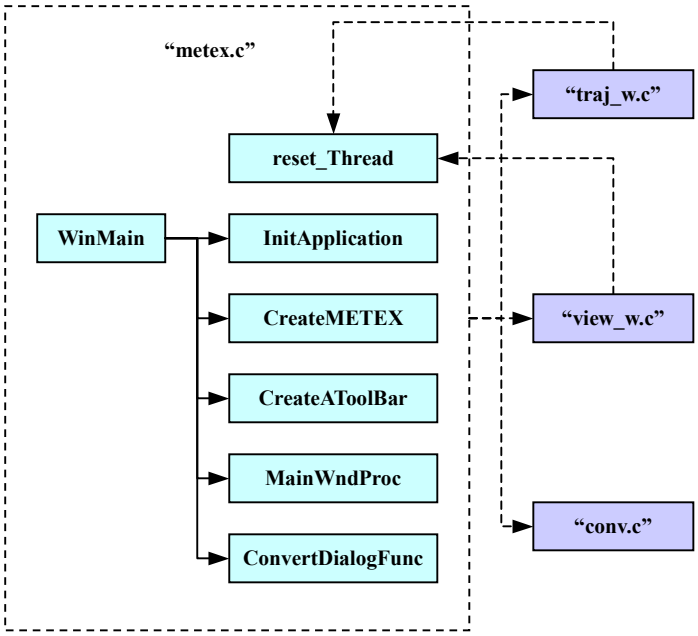

Figure 35 Function calls in “metex.c” module.

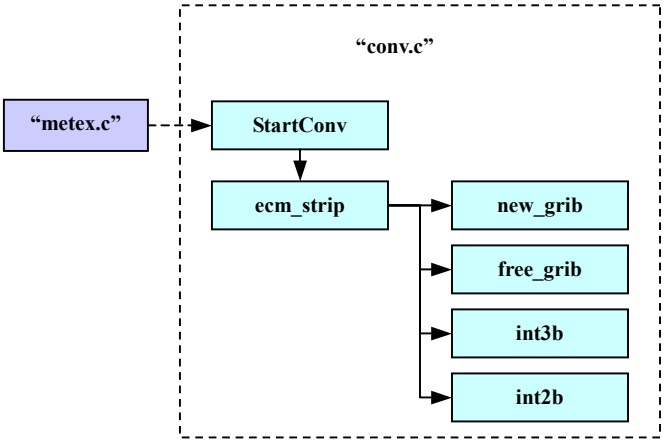

Figure 36 Function calls in “conv.c” module.

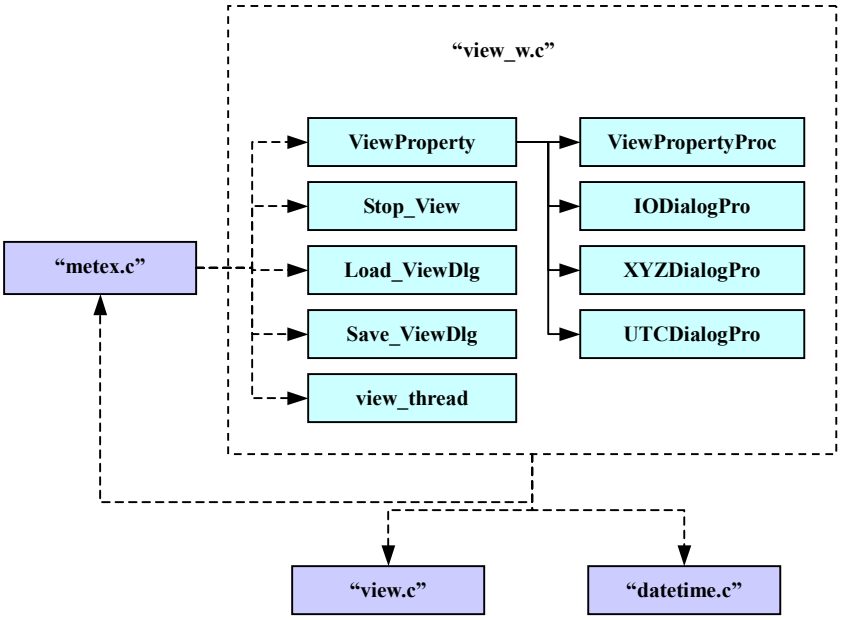

Figure 37 Function calls in "view_w.c" module.

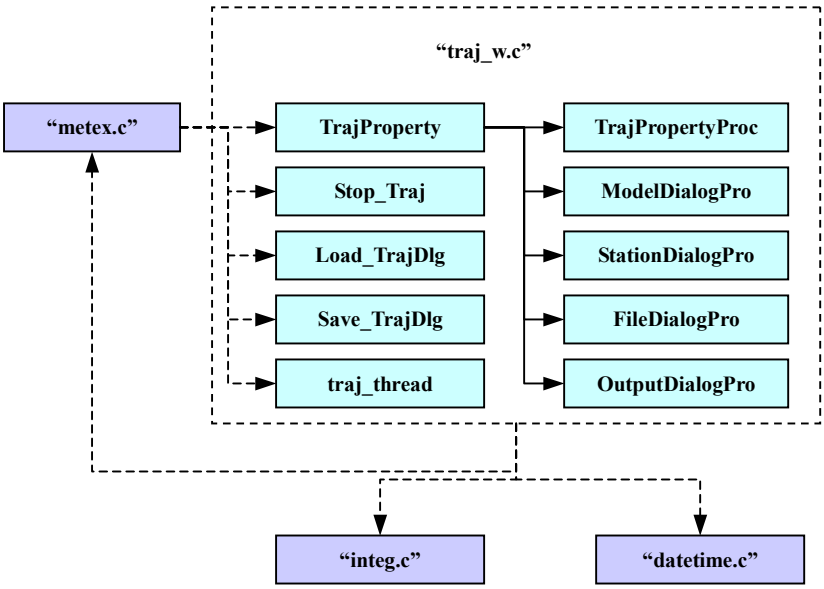

Figure 38 Function calls in "traj_w.c" module.

7.3 Trajectory Component

The trajectory tool (TRT) component is compiled as DLL in METEX. Three functions in the integration module “integ.c” are involved with the DLL: LibMain, STN_Integ, and File_Integ. The first is required by the convention of Windows DLL. It does nothing except freeing dynamically allocated memories whenever a thread or process of the trajectory program is detached from the GUI program. The functions STN_Integ and File_Integ are designated to accept initializing parameters from the GUI for the trajectory program through the IniTraj structure. The error message display function in “integ.c” is also specific to Windows.

If you intend to compile the TRT as an independent console program or to debug the program in console mode after modifications, you can supply a main function as shown below:

```
int main(void)
{
   IniTraj trj;
   trj.stop = 0;
   trj.w3d = 0;
   trj.sigma = 0;
   strcpy(trj.path_ecm,"z:¥¥metex¥¥");
   strcpy(trj.path_out,"e:¥¥temp¥¥");
   trj.par_file[0] = 0;
   strcpy(trj.gfmt,"png");
   trj.out_n = 72;
   trj.out_dt = 1. / 24.;
   trj.mode = -1;
   trj.cfl = 5;
   trj.xyt[0] = 120;
   trj.xyt[1] = 50;
   trj.xyt[2] = 50;
   trj.xyt[3] = 20;
   trj.xyt[4] = 20;
   trj.stn_x = 123.8;
   trj.stn_y = 24.05;
   trj.stn_z = 800.;
   trj.stn_dt = 0.25;
   trj.stn_t1 = 36526;    // 2000-01-01 00:00
   trj.stn_t2 = 36530;

   if (!STN_Integ(&trj)) error("Test");

   return 1;
}
```

The trajectory component involves modules of “datetime.c”, “topo.c”, “integ.c”, “ecmwf.c”, and “output.c”. Function calls in these modules are illustrated in Figure 39 to Figure 43.

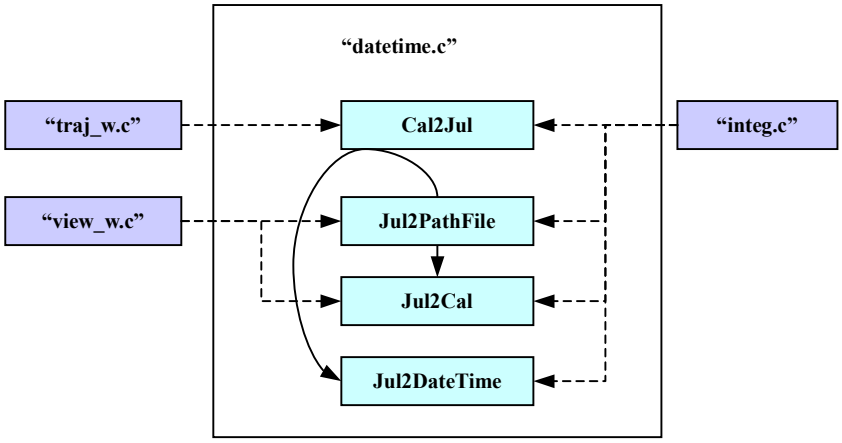

Figure 39 Function calls in "datetime.c" module.

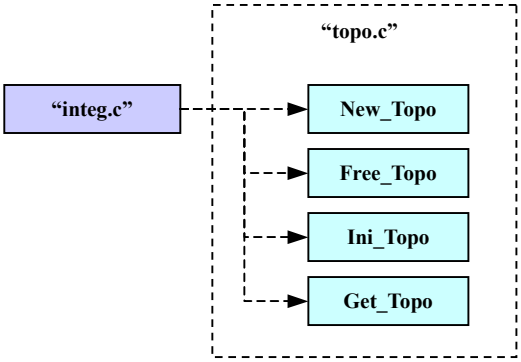

Figure 40 Function calls in "topo.c" module.

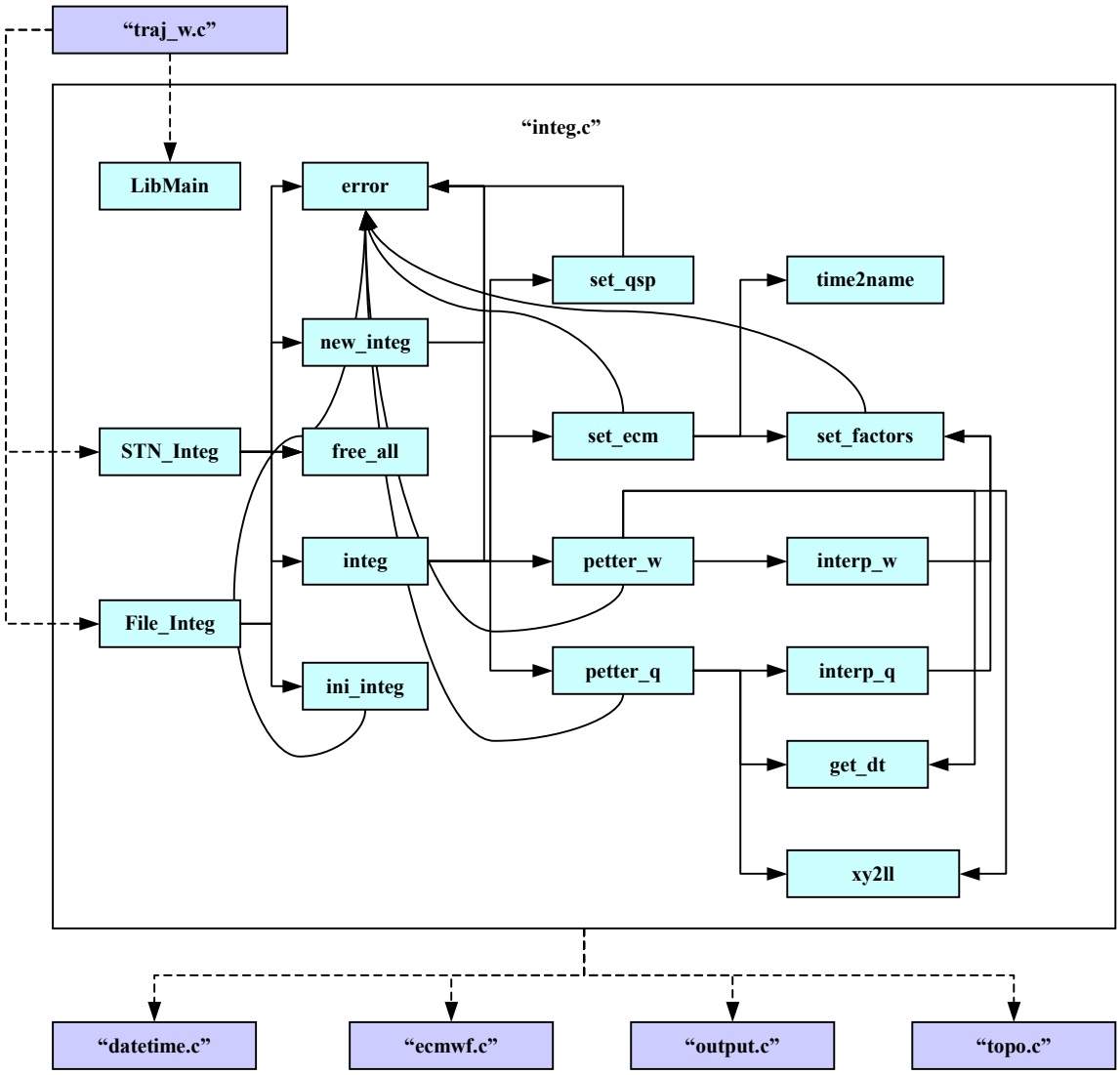

Figure 41 Function calls in "integ.c" module.

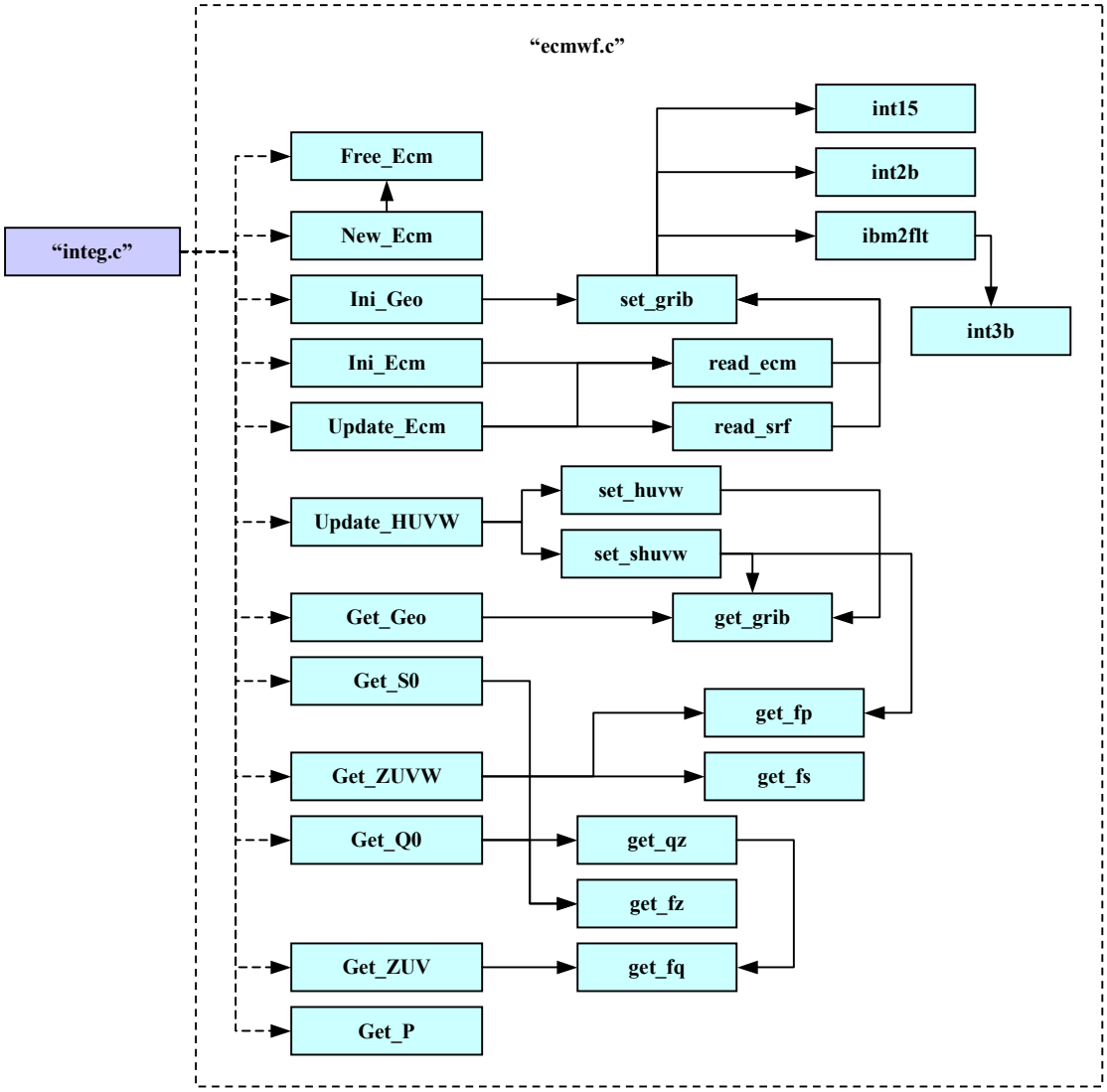

Figure 42 Function calls in "ecmwf.c" module.

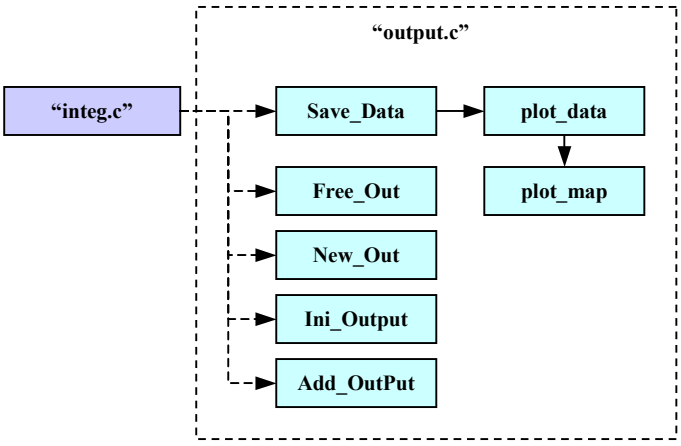

Figure 43 Function calls in "output.c" module.

7.4 Graphic View Component

The graphic viewing tool (GVT) component is also compiled as DLL in METEX. StartView is the only other DLL specific function besides the mandatory function LibMain, which includes safe guarding steps to free memory and to initialize random array pointer to null. Passing initializing parameters from GUI GVT is realized through the PLOT structure (see "view.h" in Appendix B).

If you intend to compile GVT as an independent console program or to debug the program in console mode after modifications, you can supply a main function as shown below:

```
int main(void)
{
   PLOT *plot = (PLOT*)malloc(sizeof(PLOT));
   plot->stop = 0;
   plot->csv = 0;
   strcpy(plot->ecm,"z:¥¥gmet¥¥");
   strcpy(plot->save,"e:¥¥temp¥¥");
   strcpy(plot->gfmt,"cons");
   plot->id = 2;
   plot->xyz[0] = 140;
   plot->xyz[1] = 40;
   plot->xyz[2] = 30;
   plot->xyz[3] = 10;
   plot->xyz[4] = 800;
   plot->scale[0] = 0;
   plot->scale[1] = 10;
   plot->scale[2] = 0;
   plot->scale[3] = 30;
   plot->t1 = 36526;
   plot->t2 = 36527;
   start_view(plot);
   return 1;
}
```

The graphic view component involves the “view.c” module. Function calls in the module is illustrated in

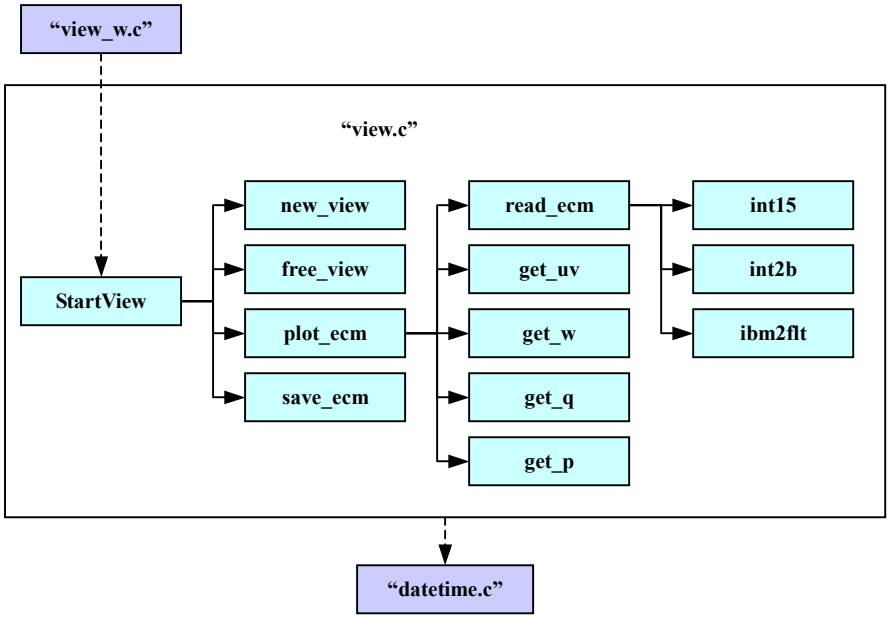

Figure 44 Function calls in “view.c” module.

Acknowledgement

The development of this program has been supported by CGER/NIES through a contract to the Global Environmental Forum. The author of the program would like to express special thanks to H. Nakane of CGER for allowing the use of STRAS for the comparison of trajectory results; and to N. Furuhashi and I. Ikeuchi of Fujitsu FIP for their great helps with GMET, STRAS, and ECMWF data.

References

Conway, T.J., Tans, P.P., Waterman, L.S., Thoning, K.W., Kitzis, D.R., Masarie, K.A. and Zhang, N. (1994) Evidence for interannual variability of the carbon cycle from the NOAA/CMDL global air sampling network, *J. Geophys. Res.*, **99**:22831-22855.

Conway, T.J. and Tans, P.P. (1999) Development of the CO_2 latitude gradient in recent decades, *Global Biogeochemical Cycles*, **13**:821-826.

Draxler, R.R. and Hess, G.D. (1998) Description of the hysplit_4 modeling system. *NOAA Tech. Memo,* ERL ARL-224, 24 pp.

Furuhashi, N. and Nakane, H. (1997) Development of a new trajectory model and its application. In: *Annual Autumn Meeting of Japan Meteorological Society*, 237 pp. (Japanese).

Haagenson, P. L., Kuo, Y.H., Skumanich, M. and Seaman, N.L. (1987) Tracer verification of trajectory models, *J. Climate Appl. Meteor*., **26**:410-426.

Harris, J.M. (1982) The GMCC atmospheric trajectory program, *NOAA Tech. Memo*, ERL-ARL-116, 30 pp.

Harris, J.M. (1992) An analysis of 5-day midtropospheric flow patterns for the South Pole: 1985-1989. *Tellus*, **44B**:409-421.

Harris, J.M. and Kahl, J.D. (1990) A descriptive atmospheric transport climatology for the Mauna Loa Observatory, using clustered trajectories. *J. Geophys. Res*., **95**:13,651-13,667.

Harris, J.M. and Kahl, J.D.W. (1994) An analysis of 10-day Isentropic Flow Patterns for Barrow, Alaska: 1985-1992, *J. Geophys. Res.,* **99**:25845-25855.

Harris, J.M., Dlugokencky, E.J., Oltmans, S.J., Tan, P.P., Conway, T.J., Novelli, P.C. and Thoning, K.W. (2000) An interpretation of trace gas correlations during Barrow, Alaska, winter dark periods, 1986-1997. *J. Geophys. Res.,* **105**:17,267-17,287.

Heffter, J.L. and Taylor, A.D. (1975) Trajectory model – Part I. A regional-continental scale transport, diffusion, and deposition model. *NOAA Tech. Memo*, ERL-ARL-50, 28 pp.

Kahl, J.D., Harris, J.M. and Herbert, G.R. (1989) Intercomparison of three long-range trajectory models applied to Arctic haze. *Tellus*, **41B**:524-536

Katsumoto, M., Furuhashi, N., Uno, I., Hayashida, S., Ide, R., Inagaki, M., Hashimoto, M., Zeng, J. and Nakane, H. (2002) Development of air mass analysis system for evaluating tropospheric monitoring data using ECMWF upper air data. CGER-M013-2002, Center for Global Environmental Research, NIES, pp.111.

Kuo, Y.-H., Skumanich, M., Haagenson, P.L. and Chang, J.S. (1985) The accuracy of trajectory models as revealed by the observing system simulation experiments, *Mon. Wea. Rev*., **113**:1852-1867.

Merrill, J.T., Bleck, R. and Avila, L. (1985) Modeling atmospheric transport to the Marshall Islands, *J. Geophys. Res.,* **90**:12927-12936.

Miller, J.M. (1981a) A five-year climatology of five day back trajectories from Barrow, Alaska. *Atmos. Environ.*, **15(8)**:1401-1405.

Miller, J.M. (1981b) A five-year climatology of five day back trajectories from the Mauna Loa Observatory, Hawaii. *Atmos. Environ.*, **15(9)**:1553-1558.

Moody, J.L. and Galloway, J.N. (1988) Quantifying the relationship between atmospheric transport and the chemical composition of precipitation on Bermuda. *Tellus*, **40B**:463-479.

Mukai, H., Katsumoto, M., Ide, R., Machida, T., Fujinuma, Y., Nojiri, Y., Inagaki, M., Oda, N. and Watai, T. (2001) Characterization of atmospheric CO_2 observed at two-background air monitoring stations (Hateruma and Ochiishi) in Japan. In: *Sixth International Carbon Dioxide Conference, Extended Abstract*, Vol.1, p108-111.

Murphy, P. P., Nojiri, Y., Fujinuma, Y., Wong, C.S., Zeng, J., Kimoto, T. and Kimoto, H. (2001) Measurements of surface seawater fCO_2 from volunteer commercial ships: Techniques and experience from Skaugran. *Journal of Atmospheric and Oceanic Technology*. **18**:1719-1734.

Nojiri, Y., Fujinuma, Y., Zeng, J. and Wong, C.S. (1999) Monitoring of pCO_2 with complete seasonal coverage

utilizing a cargo ship M/S Skaugran between Japan and Canada/US. In: Nojiri, Y. (Ed.), *Proceedings of the 2nd International Symposium of CO_2 in the Oceans*. CGER-I037-'99, p17-23.

Otomo, T., Yoshida, M., Yamamoto, H., Yamamoto, O., Kamada, M., Morishita, H. and Maeda, M. (2000) Atmospheric CO_2 concentration, Minamitorishima, in *WMO WDCGG DATA REPORT* No.25.

Pack, D.H., Ferber, G.J., Heffter, J.L., Telegadas, K., Angell, J.K., Hoecker, W.H. and Machta, L. (1978) Meteorology of long-range transport. *Atmos. Environ*., **12**:425-444.

Petterssen, S. (1940) *Weather Analysis and Forcasting*. McGraw-Hill Book Company, New York. p221-223.

Polissar, A.V., Hopke, P.K. and Harris, J.M. (2001) Source regions for atmospheric aerosol measured at Barrow, Alaska. *Environ. Sci. Technol*., **35**:4214-4226.

Stohl, A. (1999) *The flextra trajectory model*. University of Munich, Germany. 41 pp.

Thoning, K.W., Tans, P.P. and Komhyr, W.D. (1989) Atmospheric carbon dioxide at Mauna Loa Observatory 2. Analysis of the NOAA GMCC data, 1974-1985, *J. Geophys. Res*., **94**:8549-8565.

Wessel, P. and Smith, W.H.F. (1996) A global, self-consistent, hierarchical, high-resolution shoreline. *J. Geophys. Res*., **101**:8741-8743.

Contact person:

Zeng, J. Phone: (+81)29-858-1366 Facsimile: (+81)29-858-1346
E-mail: zeng@nies.go.jp